LIMNOLOGY
and
OCEANOGRAPHY

ASLO

Limnol. Oceanogr. 00, 2016, 00–00

doi: 10.1002/lno.10281

Drivers of fluorescent dissolved organic matter in the global epipelagic ocean

T. S. Catalá,*[1,2] X. A. Álvarez-Salgado,[2] J. Otero,[2] F. Iuculano,[3] B. Companys,[4] B. Horstkotte,[5] C. Romera-Castillo,[2,4] M. Nieto-Cid,[2] M. Latasa,[6] X. A. G. Morán,[6,7] J. M. Gasol,[4] C. Marrasé,[4] C. A. Stedmon,[8] I. Reche[1]

[1]Departamento de Ecología and Instituto del Agua, Universidad de Granada, Granada, Spain
[2]CSIC Instituto de Investigacións Mariñas, Vigo, Spain
[3]UIB - CSIC Instituto Mediterráneo de Estudios Avanzados, Esporles, Spain
[4]CSIC Institut de Ciències del Mar, Barcelona, Spain
[5]Faculty of Pharmacy, Charles University, Hradec Králové, Prague, Czech Republic
[6]IEO Centro Oceanográfico de Gijón/Xixón, Gijón/Xixón, Asturias, Spain
[7]Red Sea Research Center, King Abdullah University of Science and Technology, Thuwal, Saudi Arabia
[8]National Institute of Aquatic Resources, Technical University of Denmark, Charlottenlund, Denmark

Abstract

Fluorescent dissolved organic matter (FDOM) in open surface waters (< 200 m) of the Atlantic, Pacific, and Indian oceans was analysed by excitation-emission matrix (EEM) spectroscopy and parallel factor analysis (PARAFAC). A four-component PARAFAC model was fit to the EEMs, which included two humic- (C1 and C2) and two amino acid-like (C3 and C4) components previously identified in ocean waters. Generalized-additive models (GAMs) were used to explore the environmental factors that drive the global distribution of these PARAFAC components. The explained variance for the humic-like components was substantially larger (> 70%) than for the amino acid-like components (< 35%). The environmental variables exhibiting the largest effect on the global distribution of C1 and C2 were apparent oxygen utilisation followed by chlorophyll *a*. Positive non-linear relationships between both predictor variables and the two humic-like PARAFAC components suggest that their distribution are biologically controlled. Compared with the dark ocean (> 200 m), the relationships of C1 and C2 with AOU indicate a higher C1/AOU and C2/AOU ratios of the humic-like substances in the dark ocean than in the surface ocean where a net effect of photobleaching is also detected. C3 (tryptophan-like) and C4 (tyrosine-like) variability was mostly dictated by salinity (*S*), by means of positive non-linear relationships, suggesting a primary physical control of their distributions at the global surface ocean scale that could be related to the changing evaporation-precipitation regime. Remarkably, bacterial biomass (BB) only contributed to explain a minor part of the variability of C1 and C4.

Dissolved organic matter (DOM) is the largest pool of reduced organic carbon in the marine environment and is defined as the organic material that passes through a submicron filter, usually of 0.2–0.7 μm equivalent pore size (Carlson and Hansell 2015). Within this pool, the fraction that is able to absorb light over a broad range of ultraviolet (UV) and visible wavelengths is named chromophoric dissolved organic matter (CDOM). Especially in the UV and blue light region, the non-water absorption in the ocean is dominated by CDOM (Nelson and Siegel 2002), reaching more than 90% of the total absorption in the clearest waters of the South Pacific (Morel et al. 2007; Bricaud et al. 2010; Tedetti et al. 2010), and thus playing a major role in determining underwater light availability and spectral quality (Siegel et al. 1995, 2002; Nelson and Siegel 2002; Morel and Gentili 2009). Furthermore, CDOM can influence the accuracy of global satellite-based estimates of ocean chlorophyll and primary production because of its impact on the underwater light field (Siegel et al. 2005; Ortega-Retuerta et al. 2010).

In surface ocean waters, phytoplankton is the major DOM producer (Carlson 2002 and references therein). However, processes other than extracellular release by phytoplankton are also responsible for subsequent DOM production and transformation, include protistan grazer and prokaryotes release and excretion, viral cell lysis, and solubilisation of

Additional Supporting Information may be found in the online version of this article.

*Correspondence: teresascatala@gmail.com

detrital and sinking particles (Steinberg et al. 2004; Suttle 2007; Ortega-Retuerta et al. 2009; Romera-Castillo et al. 2010; Carlson and Hansell 2015). The main abiotic DOM removal process is the photochemical degradation (Mopper et al. 1991; Miller and Zepp 1995; Moran and Zepp 1997), which results in the partial or complete remineralisation of the chromophoric fraction of DOM by the absorption of light. Photodegradation plays an important role in the global biogeochemical cycles of carbon, nitrogen, sulphur, and phosphorus in the epipelagic layer (Mopper et al. 1991; Stedmon and Nelson 2015), as well as in ecological processes through the production of bioavailable substrates for microbes (Kieber et al. 1989) and in the light penetration in surface waters. Conversely, DOM exudates from phytoplankton have also been proposed as substrates for DOM photohumification, i.e., sunlight-mediated condensation from smaller molecules into polymers with higher absorption properties (Kieber et al. 1997; Reche et al. 2001). Apart from photochemical processes, heterotrophic microbes remove DOM from the water column as they incorporate and mineralise it to meet their metabolic needs. However, this is not an isolated process since they can also modify and release DOM by-products, therefore altering its optical properties (Nelson et al. 1998; Ortega-Retuerta et al. 2009).

A portion of CDOM is also able to emit fluorescence when excited by light and it was termed fluorescent dissolved organic matter (FDOM) (Kalle 1949). Recently, the spectroscopic properties of DOM have allowed tracing long-term biogeochemical processes in the global ocean (e.g., Jørgensen et al. 2011; Nelson and Siegel 2013; Catalá et al. 2015a,b; Stedmon and Nelson 2015). Excitation emission matrices (EEMs) consisting of a series of fluorescence emission spectra collected across a range of excitation wavelengths is the most common tool used to characterise FDOM in aquatic environments. Six general types of fluorescence peaks, which are usually split into two groups, have been identified in ocean waters from the EEMs (Coble 1996, 2007; Hudson et al. 2007). The amino acids tryptophan (peak T, Coble 1996), tyrosine (peak B, Coble 1996) and phenylalanine (Jørgensen et al. 2011) are included in the amino acid-like group, with Ex/Em fluorescence maxima at wavelengths of 280/350 nm, 275/305 nm, and 260/282 nm, respectively. Peak A, M, and C belong to the humic-like group and fluoresce at higher wavelengths than the amino acid-like group, with Ex/Em wavelengths of 250/435 nm, 320/410 nm, and 340/440 nm, respectively. Parallel factor analysis (PARAFAC) allows discriminating these independent fluorescent groups (or fluorophores) matching the above-mentioned peaks and tracing their distributions and changes in the environment (Stedmon and Markager 2005a). This technique disentangles the combined signal to resolve the production and degradation of FDOM in aquatic systems (Stedmon and Markager 2005b; Maie et al. 2012; Murphy et al. 2013; Jørgensen et al. 2014).

Several studies on FDOM distribution in open ocean waters have been recently published. Jørgensen et al. (2011) presented a unique global dataset of the main FDOM components, whereas other studies covered partial oceanic regions of the Atlantic (Heller et al. 2013; Kowalczuk et al. 2013; De La Fuente et al. 2014; Lønborg et al. 2015), Pacific (Kaiser and Benner 2009; Yamashita et al. 2010; Omori et al. 2011; Dainard and Guéguen 2013; Tanaka et al. 2014; Kim and Kim 2015), Indian (Coble et al. 1998), Arctic (Guéguen et al. 2007, 2014; D'Sa et al. 2014; Jørgensen et al. 2014) and Southern oceans (Yamashita et al. 2007). This study complements previous work focused on the distribution of PARAFAC components in the main water masses of the dark global ocean during the Spanish Circumnavigation Malaspina 2010 (Catalá et al. 2015a). Here, we describe the global distribution of the PARAFAC components in the illuminated global ocean by parcelling it in Longhurst's biogeographic provinces, analysing the variability of the fluorescence components among and within provinces and determining the environmental drivers controlling their distribution.

Materials and methods

Division of the epipelagic layer into Longhurst's biogeographic provinces

The Malaspina 2010 circumnavigation was conducted from December 2010 to July 2011 on board R/V *Hespérides* along the Atlantic, Indian, and Pacific oceans, spanning latitudes from 34°N to 40°S (Fig. 1). To expedite the study of the FDOM distribution in the surface ocean, the Malaspina cruise track was parcelled according to Longhurst's biogeographic provinces. This partition is based on physical forces in ocean and atmosphere (i.e., turbulence, temperature, irradiance, and nutrients) that affect phytoplankton distribution (Longhurst 1995, 1998). According to this division, four domains can be recognised in every ocean basin: Polar, Westerlies, Trade-Winds, and Coastal Boundary Zone. At the second level of resolution, the ocean basins are partitioned into 56 biogeographic provinces (Ducklow 2003).

A total of 147 stations were assigned to 15 Longhurst's biogeographic provinces (distinguished by green colour in Fig. 1) according to their geographical coordinates, covering all the domains except the Polar (Fig. 1). Six provinces were in the Atlantic Ocean, four in the Indian Ocean; and five provinces in the Pacific Ocean (acronyms described in Table 1; Fig. 1). The provinces NASE and NATR were sampled in winter (NASE_W, NATR_W) and summer (NASE_S and NATR_S). An exhaustive analysis of the vertical profiles of salinity, potential temperature, dissolved oxygen and fluorescence of chlorophyll *a* (Chl *a*) was performed in the stations closer to the boundary between two provinces to place them in the appropriate province.

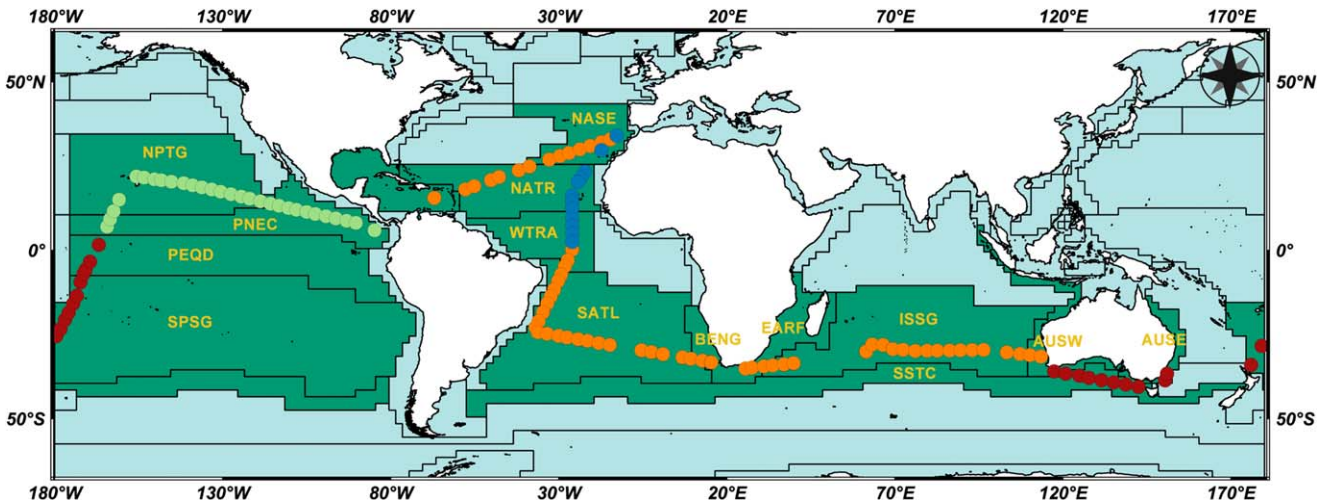

Fig. 1. Map of the biogeographic provinces crossed during the Malaspina 2010 circumnavigation. NASE, North Atlantic Subtropical Gyral; NATR, North Atlantic Tropical Gyral; WTRA, Western Tropical Atlantic; SATL, South Atlantic Gyral; BENG, Benguela Current Coastal Province; EARF, East Africa Coastal; ISSG, Indian South Subtropical Gyre; SSTC, South Subtropical Convergence; AUSE, East Australian Coastal Province; SPSG, South Pacific Subtropical Gyre; PEQD, Pacific Equatorial Divergence; NPTG, North Pacific Tropical Gyre; PNEC, North Pacific Equatorial Countercurrent; CARB, Caribbean Province. Circles indicate the position of the 147 stations sampled during the circumnavigation. The colour of the circles account for the season: blue (winter), orange (summer), red (autumn), green (spring).

Data acquisition

On each of the 147 sampling days of the circumnavigation a rosette sampler equipped with 24 Niskin bottles of 10 L was dipped at about 10:00 a.m. (local time) to collect water samples in the epipelagic layer (< 200 m). Seven nominal levels were sampled coinciding with the 70%, 20%, and 7% of photosynthetically active radiation (PAR), deep chlorophyll maximum (DCM), DCM plus 20 m (DCM+20), DCM plus 50 m (DCM+50), and 200 m. For Chl *a*, only samples at 70%, 20%, and 7% of PAR, DCM, and DCM+20 were collected. For bacterial biomass, only samples at 20% and 7% of PAR, DCM, and DCM+20 were collected. Vertical profiles of salinity (S), potential temperature (θ), dissolved oxygen (O_2), in vivo fluorescence of Chl *a* (FISP) and PAR were recorded continuously with a conductivity–temperature–depth (CTD) probe Seabird 911+, a polarographic membrane oxygen sensor Seabird SBE-43, a fluorometer Seapoint and a radiometer Biospherical/Licor installed in the rosette sampler. The CTD was equipped with redundant temperature and salinity sensors for intercomparison during the cruise. Temperature and pressure sensors were calibrated at the SeaBird laboratory before the cruise. On board salinity calibration was carried out with a Guildline AUTOSAL model 8410B salinometer (Pérez-Hernández et al. 2012), the potentiometric end-point Winkler method for the calibration of the oxygen sensor (Álvarez et al. 2012) and the fluorimetric method for the calibration of the fluorescence of Chl *a* profiles (Estrada 2012). The squared Brunt-Väisälä frequency (N^2), commonly used to quantify the stratification of the water column, was calculated following Millard et al. (1990):

$$N^2 = -\frac{g}{\rho}\cdot\frac{\partial\rho}{\partial z} = -g\cdot\frac{\partial \ln(\rho)}{\partial z} \quad (1)$$

where g is the gravity acceleration constant (9.8 m s^{-2}), z is the water depth, and ρ is the water potential density at depth z. Integration of Eq. 1 between two depth levels (1 and 2): $\bar{N}^2 = -g\cdot\ln(\rho_2/\rho_1)/(z_2-z_1)$, provides a measure of the average stability of the water column between z_1 and z_2 (Lønborg et al. 2015). Here, we have calculated N^2 between the 70% PAR (3 m) and 150 m. Furthermore, we have also calculated the gradients of potential temperature and salinity ($D\theta$ and DS) over the upper 150 m, which were obtained as the difference between the potential temperature or salinity at 70% PAR (about 3 m) and 150 m divided by the difference in depth (147 m). The mixed layer depth (MLD) was calculated as the depth where potential density exceeded the value at 3 m by 0.1 kg m^{-3} (Fernández-Castro et al. 2014). Daily, weekly and monthly short wave (wavelength range, 175–3850 nm) solar radiation data (SWR, in MJ m^{-2} d^{-1}) were obtained from the National Centres for Environmental Predictions NCEP/DOE 2 reanalysis database provided by the NOAA/OAR/ESRL PSD, Boulder, Colorado, U.S.A., (http://www.esrl.noaa.gov/psd/) and interpolated for each station. Apparent Oxygen Utilization (AOU) was calculated as the difference between the saturation and measured dissolved oxygen concentrations. Dissolved oxygen saturation was calculated from practical salinity and potential temperature with the equation of Benson and Krause (1984). Inorganic nutrients (nitrate, phosphate and silicate) were collected from the Niskin bottles in 20-mL acid-washed polyethylene flasks and determined on board using standard segmented

Table 1. Averages and standard deviations of potential temperature (θ, °C), salinity (S), weekly short wave radiation (SWR, MJ m^{-2} d^{-1}), apparent oxygen utilization (AOU, μmol kg^{-1}), chlorophyll *a* (Chl *a*, μg L^{-1}) and bacterial biomass (BB, μg C L^{-1}) of the biogeographic provinces intercepted during the Malaspina 2010 expedition.

Province CODE	Province description	Biome	Sampling date (yymmdd)	Stations	θ (°C)	S (pss)	Weekly SWR (MJ m^{-2} d^{-1})	AOU (μmol kg^{-1})	Chl *a* (μg L^{-1})	BB (μg C L^{-1})
CARB	Caribbean Province	T	110623	130 (Leg 7)	-	-	-	-	-	-
NATR	N. Atlantic Tropical Gyral Province (TRPG)	T	Summer: 110626-110703	132-139 (Leg 7)	23.6 ± 1.8	37.1 ± 0.3	24.0 ± 1.2	3.3 ± 6.8	0.19 ± 0.06	3.7 ± 1.1
			Winter: 101222-101227	6-11 (Leg 1)	22.1 ± 1.5	36.4 ± 0.5	14.5 ± 3.0	45.0 ± 25.9	0.30 ± 0.09	3.7 ± 1.1
NASE	N. Atlantic Subtropical Gyral Province (East) (STGE)	W	Summer: 110705-110711	141-147 (Leg 7)	20.2 ± 1.0	36.8 ± 0.2	21.5 ± 1.6	0.0 ± 3.7	0.17 ± 0.07	3.3 ± 0.7
			Winter: 101217-101219	2,3 (Leg 1)	-	-	-	-	-	-
WTRA	Western Tropical Atlantic Province	T	101228-110103	12-18 (Leg 1)	20.0 ± 1.4	35.7 ± 0.2	22.5 ± 2.3	71.1 ± 17.8	0.40 ± 0.14	5.4 ± 1.5
SATL	South Atlantic Gyral Province (SATG)	T	110104-110202	19-41 (Leg 1, 2)	20.7 ± 2.3	36.3 ± 0.4	25.0 ± 3.5	2.0 ± 15.0	0.19 ± 0.05	2.6 ± 0.8
BENG	Benguela Current Coastal Province	C	110203-110205	42-44 (Leg 2)	-	-	-	-	-	-
EARF	E. Africa Coastal Province	C	110213-110215	45-47 (Leg 3)	-	-	-	-	-	-
ISSG	Indian S. Subtropical Gyre Province	T	110216-110309	48-65 (Leg 3)	18.7 ± 1.3	35.6 ± 0.1	21.5 ± 2.4	2.8 ± 5.3	0.16 ± 0.06	3.6 ± 1.4
AUSW	Australia-Indonesia Coastal Province	C	110310-110319	66-69 (Leg 3, 4)	18.7 ± 1.8	35.6 ± 0.2	20.0 ± 5.0	6.1 ± 3.1	0.22 ± 0.09	4.2 ± 1.6
SSTC	S. Subtropical Convergence Province	W	110320-110326	70-76 (Leg 4)	14.2 ± 0.9	35.2 ± 0.1	16.7 ± 2.6	6.2 ± 4.0	0.24 ± 0.10	6.3 ± 2.7
AUSE	East Australian Coastal Province	C	110328-110329	77, 78 (Leg 4)	-	-	-	-	-	-
SPSG	S. Pacific Subtropical Gyre Province	T	110417-110426	79-89 (Leg 5)	24.3 ± 2.8	35.5 ± 0.3	18.9 ± 1.6	16.6 ± 8.2	0.23 ± 0.05	2.7 ± 1.5
PEQD	Pacific Equatorial Divergence Province	T	110427-110504	90-97 (Leg 5)	23.5 ± 3.6	35.2 ± 0.5	23.4 ± 2.9	49.9 ± 40.4	0.27 ± 0.05	5.2 ± 2.3
NPTG	N. Pacific Tropical Gyre Province	T	110505-110523	98-110 (Leg 5, 6)	21.4 ± 1.7	34.8 ± 0.3	21.8 ± 6.6	12.6 ± 11.2	0.24 ± 0.09	5.0 ± 1.4
PNEC	N. Pacific Equatorial Countercurrent Province	T	110529-110608	116-126 (Leg 6)	17.1 ± 2.3	34.6 ± 0.2	19.1 ± 2.3	176.1 ± 43.6	0.36 ± 1.18	6.3 ± 2.8

We have not calculated the average and standard deviation of biogeographic provinces with less than 4 stations.
C, Coastal; T, Trades; W, Westerlies.

flow analysis methods with colorimetric detection (Blasco et al. 2012).

Bacterial biomass (BB) was determined by flow cytometry using standard protocols after fixation with 1% paraformaldehyde and 0.05% glutaraldehyde and staining with Sybr-Green I (Molecular Probes, Invitrogen) at a 1/10,000 dilution (Gasol and del Giorgio 2000). A previously published calibration curve relating relative side scatter to cell size (Calvo-Díaz and Morán 2006) was used to transform the cytometric signal. Cell size was converted to biomass using the Gundersen et al. (2002) relationship.

Collection and spectral acquisition of fluorescent DOM samples

We collected 835 water samples for FDOM measurements. They were transferred from the Niskin bottles into 250 mL acid-washed glass flasks and stored in dark conditions until measurement before 6 h from collection. Once in the on board laboratory, aliquots were immediately filtered through precombusted (450°C, 4 h) glass fibre filters (GF/F) in an acid-cleaned all-glass filtration system, under positive pressure with low N_2 flow.

Fluorescence EEMs were collected with a JY-Horiba Spex Fluoromax-4 spectrofluorometer at room temperature (around 20°C) using 5 nm excitation and emission slit widths, an integration time of 0.25 s, an excitation range of 240–450 nm at 10 nm increments, and an emission range of 300–560 nm at 2 nm increments. To correct for lamp spectral properties and to compare results with those reported in other studies, spectra were collected in signal-to-reference (S:R) mode with instrument-specific excitation and emission corrections applied during collection, and EEMs were normalized to the Raman area (RA). In our case, RA normalization and its baseline correction were performed with the emission scan at 350 nm of the Milli-Q water blanks and the area was calculated following the trapezoidal rule of integration (Murphy et al. 2010).

Furthermore, to verify that the variability of the instrument during the 147 working days of the expedition affected similarly to the Raman, amino acid and humic-like regions of the spectrum, the following three standards were run daily: (1) a sealed Milli-Q cuvette (Perkin Elmer) scanned between 365 nm and 450 nm exciting at 350 nm; (2) a P-terphenyl block (Stranna) that fluoresces in the amino acid region, between 310 nm and 600 nm exciting at 295 nm; and (3) a Tetraphenyl butadiene block (Stranna) that fluoresces in the humic region, between 365 nm and 600 nm exciting at 348 nm. Successful Raman normalization in both the amino acid- and humic-like regions of the EEMs, a good quality of the Milli-Q water produced on board and a slight shift of fluorescence intensities on daily working routine were observed (see Supporting Information in Catalá et al. 2015a).

Inner-filter correction was not applied due to the low absorption coefficient of CDOM of the epipelagic water samples collected during the circumnavigation: 1.31 ± 0.23 m^{-1} (average ± standard deviation) at 250 nm, i.e., much lower than the threshold of 10 m^{-1} above which this correction is required (Stedmon and Bro 2008). Raman-normalized Milli-Q blanks were subtracted to remove the Raman scattering signal (Stedmon and Markager 2003; Murphy et al. 2010). Raman Area (RA) normalization, blank subtraction, and generation of EEMs were performed using MATLAB (version R2008a).

Global PARAFAC modelling

Parallel factor analysis (PARAFAC) was used to identify the different fluorescent components that comprise the EEMs in the epipelagic waters of the global ocean. PARAFAC was performed using the DOMFluor 1_7 Toolbox (Stedmon and Bro 2008). Prior to the analysis, Rayleigh scatter bands (first order at each wavelength pair where Em= Ex ±bandwidth; second order at each wavelength pair where Em=2∗Ex ±(2∗bandwidth)) were trimmed. This PARAFAC model was derived from the global PARAFAC model based on the 1574 corrected EEMs collected during the circumnavigation from the surface to 4000 m depth and was validated using split-half validation and random initialization (Stedmon and Bro 2008). Likewise, we also tested the PARAFAC model using the subset of 835 epipelagic water samples (surface to 200 m) and it turned out in a similar components model. Here we report the fluorescence intensities in Raman units (RU) (Stedmon et al. 2003; Murphy et al. 2010).

Statistical analysis

Intra-province variability: ANOVA

To determine the relevance of intra-province variability for each environmental variable and fluorescent component among PAR levels we performed an analysis of variance (ANOVA). The provinces CARB, NASE_W, BENG, EARF and AUSE were excluded because they comprised less than 4 stations.

Drivers of fluorescence components: generalised additive models (GAMs)

To test for the effect of the environment on the variability of the fluorescence PARAFAC components we used generalized additive models (GAMs, Wood 2006). We examined the influence of 11 environmental predictors on each fluorescence component: SWR (i.e., daily, weekly and monthly), S, θ, N^2, DS, Dθ, O_2, AOU, Chl a, NO_3^- and BB. Before model fitting, covariability among predictors was examined using variance inflation factors (VIFs, Supporting Information Table S1); and the selection among daily, weekly and monthly SWR was on basis of minimizing the AIC (Akaike Information Criterion) and the GCV (Generalized Cross Validation). GAMs were formulated as follows:

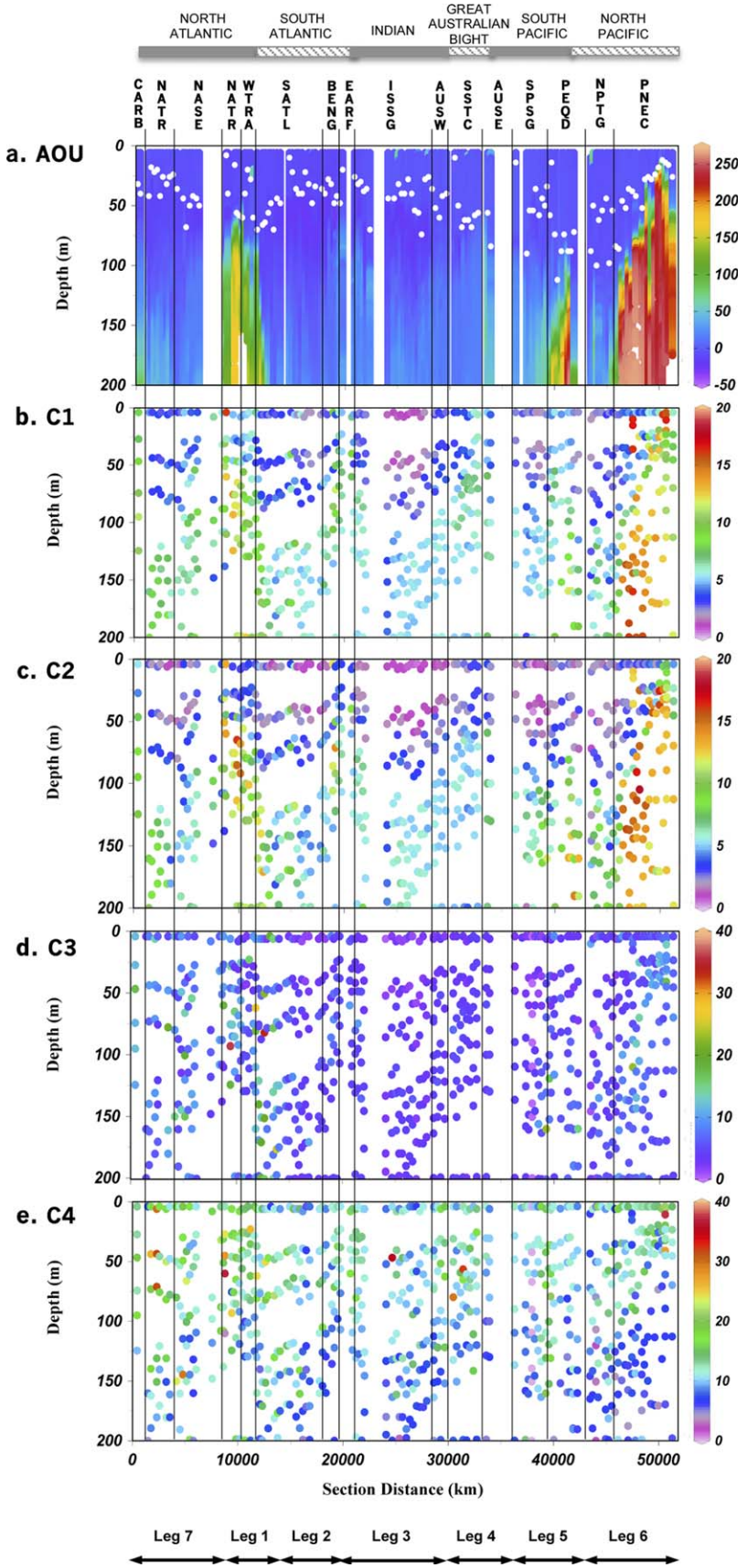

Fig. 2. Distribution of the apparent oxygen utilization (AOU) (μmol Kg^{-1}) (a), and the components C1 (10^{-3}, RU) (b), C2 (10^{-3}, RU)(c), C3 (10^{-3}, RU) (d) and C4 (10^{-3}, RU) (e) delivered by Parallel Factor Analysis (PARAFAC) during the Malaspina 2010 expedition. The black vertical lines show the biogeographic provinces delimitations. Provinces acronyms are described in Table 1. White dots in the upper panel represent the mixed layer depth (MLD).

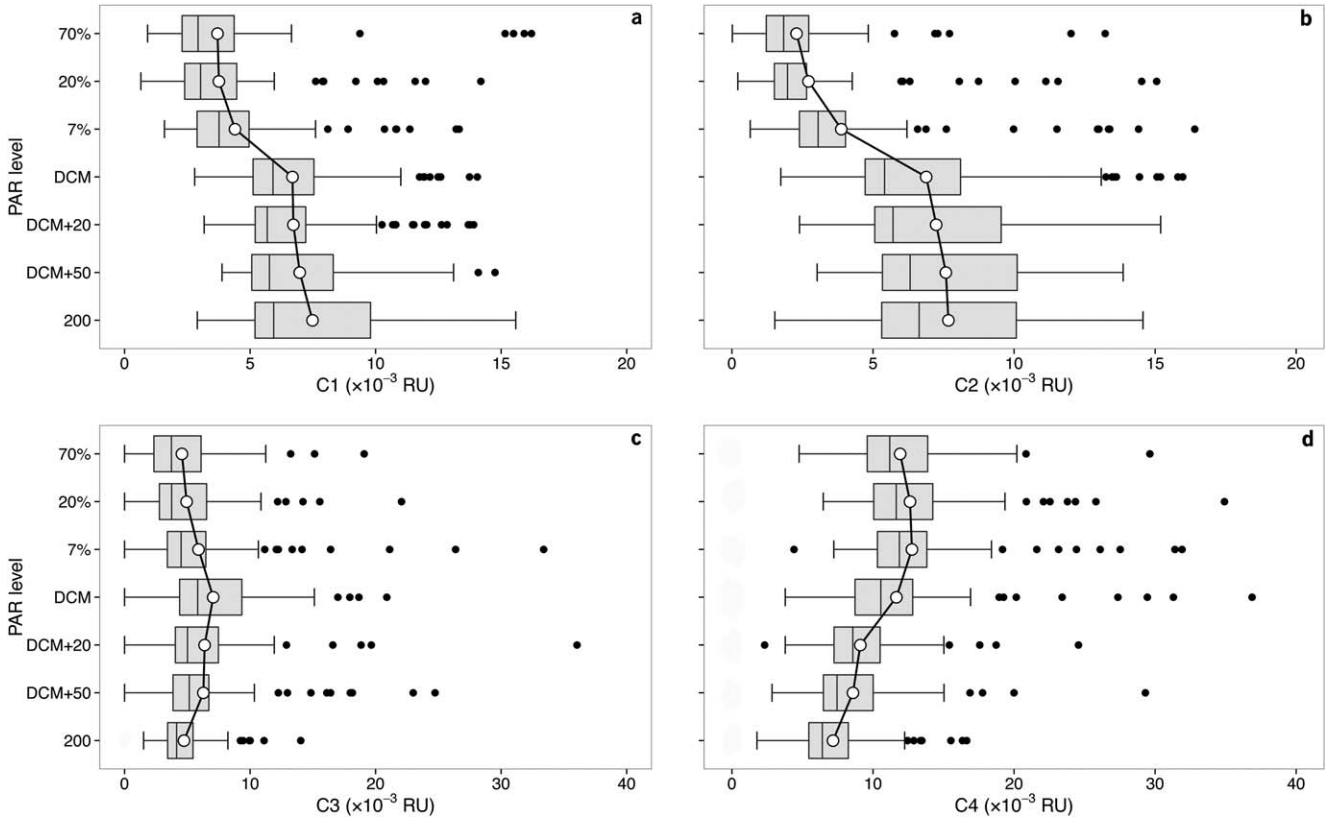

Fig. 3. Average profiles of the four PARAFAC components C1 (**a**), C2 (**b**), C3 (**c**) and C4 (**d**) for each nominal depth in the epipelagic ocean. Horizontal line, median; white dots, mean; gray-box, 25–75% percentiles; and whiskers extend from the upper (lower) to the highest (lowest) value that is within 1.5 × inter-quartile range of the hinge.

$$Y_{i,l} = \alpha + \sum_j g_j\left(X^j_{i,l}\right) + \in_{i,l} \quad (2)$$

where Y is a fluorescence PARAFAC component measured at a station i and depth level l, α is an intercept, X is a vector of predictor variables where the superscript j identifies each covariate, g is a non-parametric smoothing function specifying the effect of each covariates on the fluorescent component and $\in_{i,l}$ is the error term assumed to be normally distributed. Smoothing functions were fit by penalized cubic regression splines restricted to a maximum of three knots. The smoothness of the functions was estimated by minimizing the generalized cross validation criterion. Given that BB was measured in 473 of the 835 samples, two models were run for each fluorescence component: first, models were obtained with all predictor variables but BB; and second models were obtained with all predictor variables including BB. In the second case, to test for the effect of reducing the dataset by about a half, the models were run for all predictor variables but BB considering only the samples where BB was measured.

Chl *a* and BB were ln-transformed, and depth was included in all models as a "catch-all" variable to account for potential unmeasured effects on fluorescence. All models were fitted in R 3.1.1 software (R Development Core Team 2014) and using the 'mgcv 'mgcv 1.8-0' package (Wood 2006).

Regression analysis: parametric relationships

Non-linear power-law regression equations between AOU and each fluorescent component (C1, 2, 3, and 4) were fitted in R 3.1.1 software.

Results

PARAFAC components

A four-component model was obtained (Supporting Information Fig. S1), two of them of humic-like nature—C1 and C2—since they display a broad emission spectra around 400 nm, at Ex/Em < 270–370/470 nm and Ex/Em 320/400 nm, respectively, and two of amino acid-like nature—C3 and C4—as the emission spectra is narrower with maxima below 400 nm at 290/340 nm and 270/310 nm, respectively. In the literature, the humic-like C1 and C2 have been defined as Peak A/C and peak M, respectively (Coble 1996). C1 is proposed to be ubiquitous in DOM but enriched in terrestrial/allochthous sources (Stedmon and Markager 2005a). C2 has previously been reported as marine humic-like

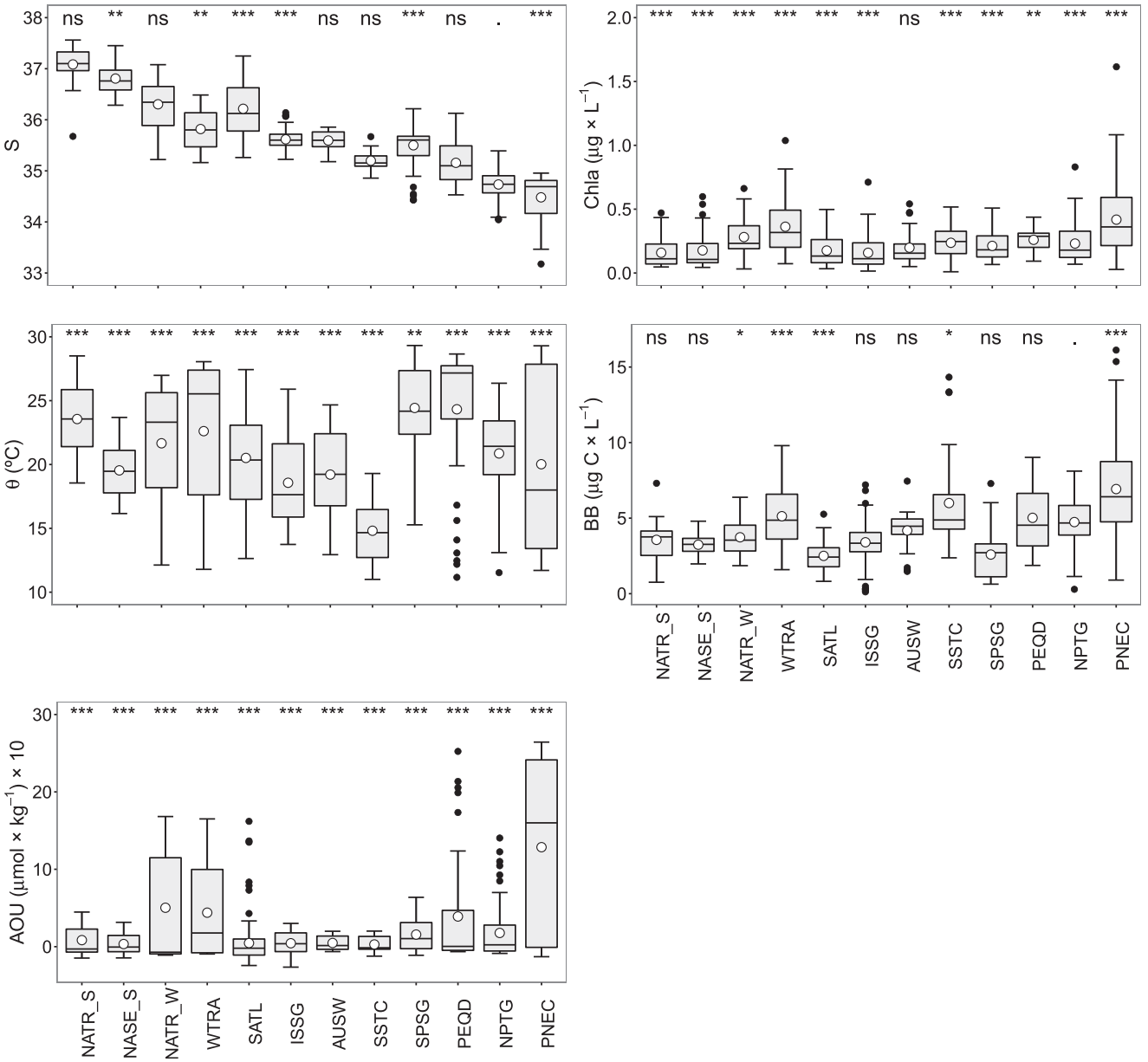

Fig. 4. Box and Whisker plots and *p*-value of the *F*-statistic test resulting from the use of ANOVA applied to the five physical, chemical and biological variables at each biogeographic province. Horizontal line, median; white dots, mean; gray-box, 25–75% percentiles; and whiskers extend from the upper (lower) to the highest (lowest) value that is within 1.5 × inter-quartile range of the hinge. n.s.: non significant, indicative of homogeneity in average differences in environmental variables among PAR depth levels within a specific province; ns = $p > 0.05$, $p < 0.05$, *$p < 0.01$, **$p < 0.001$, ***$p < 0.0001$.

substances (Coble 1996). Both humic-like components appear to be photodegradable but biorefractory (Maie et al. 2012). The amino acid-like C3 and C4 have been attributed to tryptophan and tyrosine, which have been shown to represent more biodegradable and fresher microbially produced DOM (Yamashita and Tanoue 2003a; Fellman et al. 2008) and have been commonly termed as peaks T and B (Coble 1996), respectively. These four peaks are recurrently observed in diverse aquatic environments (e.g., Stedmon and Markager 2005a; Yamashita et al. 2008; Jørgensen et al. 2011; Maie et al. 2012; Catalá et al. 2015a).

The global average vertical profiles (Figs. 2, 3) reveal distinct patterns with depth for the PARAFAC components. Whereas C1 (Figs. 2b, 3a) and C2 (Figs. 2c, 3b) increased with depth, C4 (Fig. 3d) exhibited the opposite trend. C3 (Fig. 3c) showed an intermediate behaviour, with maximum values at the depth of the DCM (average ± SD depth, 95 ± 36 m) and minimum either at the surface or 200 m.

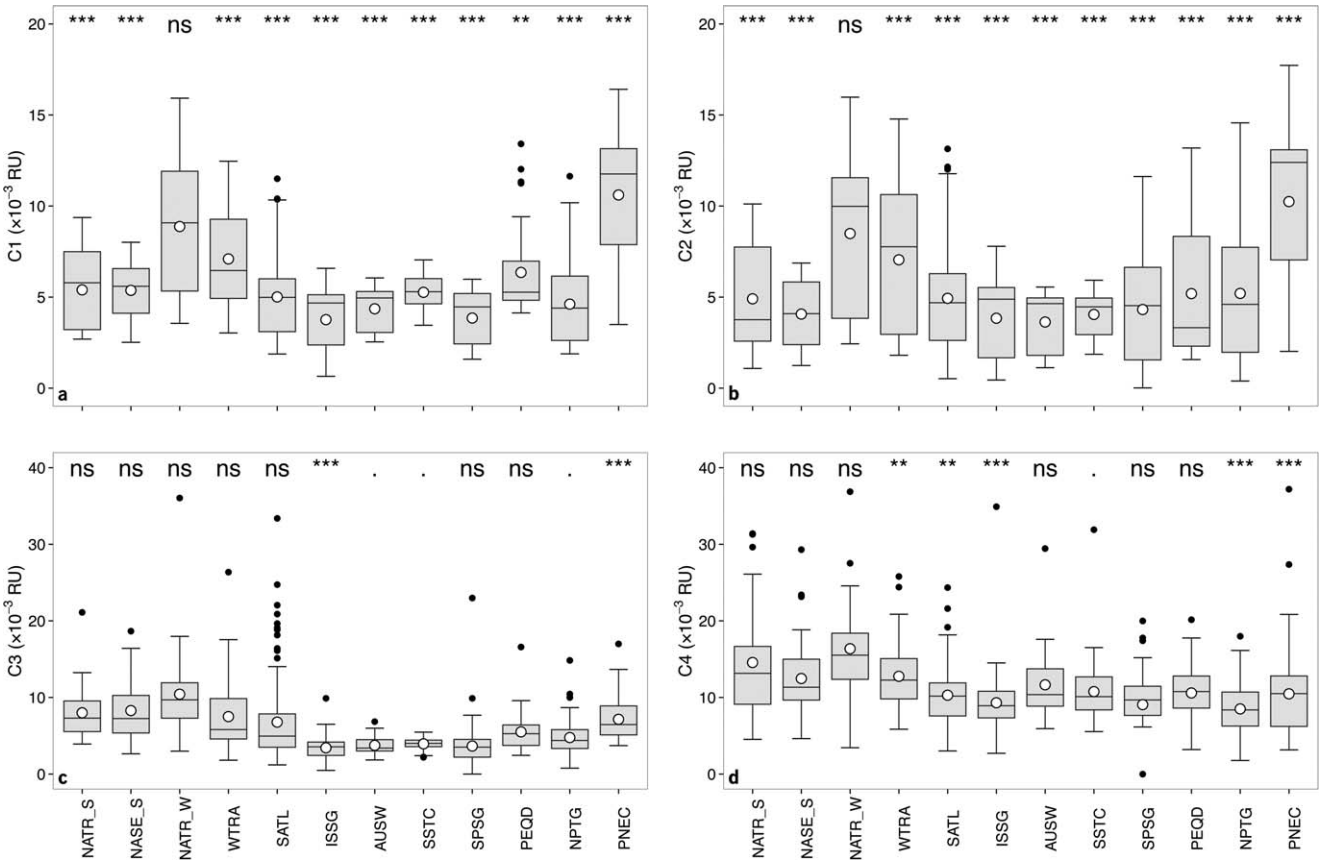

Fig. 5. Box and Whisker plots and *p*-value of the *F*-statistic test resulting from the use of ANOVA applied to the four fluorescent components at each biogeographic province. Horizontal line, median; white dots, mean; gray-box, 25–75% percentiles; and whiskers extend from the upper (lower) to the highest (lowest) value that is within 1.5 × inter-quartile range of the hinge. n.s.: non significant, indicative of homogeneity in average differences in fluorescent components among PAR depth levels within a specific province; ns = $p > 0.05$, $p < 0.05$, *$p < 0.01$, **$p < 0.001$, ***$p < 0.0001$.

Differences among biogeographic provinces

The mean and standard deviation of all study variables was calculated for each biogeographic province and nominal depth level (70%, 20%, 7% PAR, DCM, DCM+20, and DCM+50). Salinity profiles were very homogeneous in all the study provinces with maximum values about 37 in NASE and NATR during summer and minimum values of about 34 in PNEC (Fig. 4a, Supporting Information Figs. S2a, S3a). Potential temperature, which ranged from 11°C to 29°C, showed very homogeneous profiles in some provinces such as NASE and NATR_S or strongly stratified profiles in other provinces such as PNEC, WTRA, or NATR_W (Fig. 4b, Supporting Information Figs. S2b, S3b). DS ranged between −0.005 and −0.012 m^{-1} (Supporting Information Fig. S4a) and the maximum was found in NASE_S whereas the minimum in PNEC. Dθ ranged between −0.115°C m^{-1} and −0.010°C m^{-1} (Supporting Information Fig. S4b) and the highest values were found in PNEC and the minimum in NASE. MLD ranged from 8 m to 100 m, with an average ± SD of 48 ± 21 m (Fig. 2a). The maximum values were found in NPTG whereas the minimum was found in EARF and PNEC. The weekly SWR ranged from 11 MJ m^{-2} d^{-1} to 31 MJ m^{-2} d^{-1} (Supporting Information Fig. S4c). SATL (occupied in summer) underwent the maximum average weekly SWR with 25 ± 3 MJ m^{-2} d^{-1}, followed by EAFR (occupied in summer) with 25 ± 1 MJ m^{-2} d^{-1}. NASE (occupied in winter) showed the lowest average weekly SWR with 11 MJ m^{-2} d^{-1}. N^2 ranged from 0.1 to 1.2 min^{-2} (Supporting Information Fig. S4d), with PEQD showing the maximum and NASE_S the minimum values. AOU ranged from −26 μmol kg^{-1} to 266 μmol kg^{-1} (Figs. 2a, 4c, Supporting Information Fig. S2c). The maximum values were found in PNEC between 100 m and 200 m depth, whereas the minimum values were located between 50 m and 75 m depth in the South Atlantic and South Indian oceanic gyres, corresponding to the provinces SATL and ISSG (Figs. 2a, 4c, Supporting Information Fig. S2c). AOU increased with depth in all provinces; the AOU in the mixed layer showed negative values for all stations, except in PNEC (Figs. 2a, 4c), highlighting the predominance of primary production against respiration.

Chl *a* ranged from 0.01 μg L^{-1} to 1.93 μg L^{-1} and the deep DCM was located between 37 m and 161 m (Fig. 4d, Supporting Information S2d, S3c). Maximum Chl *a* values were found in NATR and PNEC whereas the minima were in

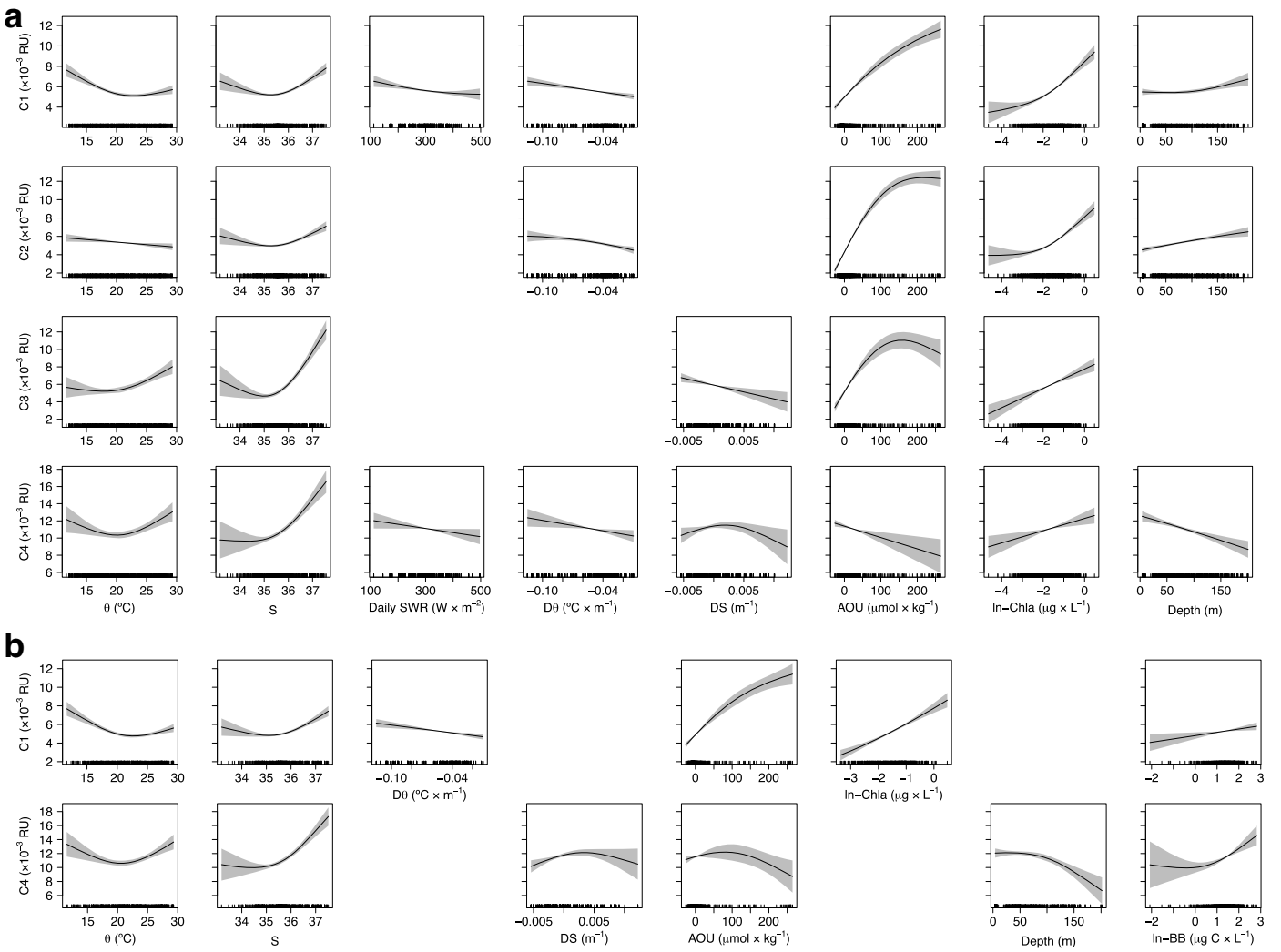

Fig. 6. Partial plots of two models showing the additive effects of the physical, chemical and biological covariates on the four fluorescent components (**a**) by excluding the bacterial biomass ($n = 835$) and (**b**) by including the bacterial biomass ($n = 473$). The orange lines are the smoothing functions and the blue shaded areas represent 95% point-wise confidence intervals. Rugs on *x*-axis indicate the distribution of the data.

the centre of the oceanic gyres. The maximum depths of the DCM were coincident with the centre of the oceanic gyres and were located in the SATL, ISSG, and NPTG. BB ranged from 0.1 μg C L^{-1} to 16.7 μg C L^{-1} and the maxima were found in SSTC and PNEC (Fig. 4e, Supporting Information Fig. S3d). The minimum values were not found in a specific geographic area, although a noticeable group of samples with values near 0 was found around 150 m in the SATL (Fig. 4e, Supporting Information Fig. S3d).

The humic-like components C1 and C2 presented fluorescent values ranging from 0.6 to 17.2 $\times$ 10^{-3} RU and from below detection limit to 17.7 $\times$ 10^{-3} RU, respectively, and their distributions concurred with the AOU distribution (Fig. 2a,b,c, Supporting Information Fig. S2c,e,f). The maximum averages of C1 and C2 were 11.5 $\pm$ 1.8 and 11.6 $\pm$ 1.8 $\times$ 10^{-3} RU, respectively and were found at the PNEC province (Fig. 5a,b). The ISSG and SPSG provinces showed the minimum means of C1, with values of 3.7 $\pm$ 0.6 and 4.0 $\pm$ 0.5 $\times$ 10^{-3} RU (Fig. 5a). The lowest C2 means were found in ISSG and NASE_S with 3.8 $\pm$ 0.6 $\times$ 10^{-3} RU (Fig. 5b).

The amino acid-like components C3 and C4 were generally twice more intense than the humic-like components (Fig. 3); C3 ranged from below detection limit to 36.0 $\times$ 10^{-3} RU and C4 from below detection limit to 37.2 $\times$ 10^{-3} RU, respectively (Fig. 3). C3 was nearly absent in some oceanic areas such as the South Atlantic, the South Indian Ocean or the South Pacific, corresponding to the provinces AUSW, SSTC, ISSG, and SPSG (Figs. 2c, 5c, Supporting Information Fig. S2g); C4 was the most homogeneously distributed component with a C4 difference of around 10 $\times$ 10^{-3} RU throughout the water column (Figs. 2e, 5d, Supporting Information Fig. S2h). The NATR_W province presented the maximum average for C3 and C4, 11.5 $\pm$ 6.0 and

$17.2 \pm 0.7 \times 10^{-3}$ RU (Fig. 5c,d), respectively, whereas the lowest means were $3.5 \pm 1.1 \times 10^{-3}$ RU at ISSG for C3 (Fig. 5c) and $8.5 \pm 2.3 \times 10^{-3}$ RU at PNEC for C4 (Fig. 5d).

Differences within biogeographic provinces

ANOVAs among the different depth levels were used to explore the variability of the environmental parameters (Fig. 4) and the four PARAFAC components in each province (Fig. 5). θ, AOU and Chl *a* had significant intra-province differences (Fig. 4b,c,d, Supporting Information Fig. S2b,c,d). Salinity was not as variable as the previous parameters and the provinces NATR_S, NATR_W, AUSW, SSTC and PEQD were homogeneous with depth (Fig. 4a, Supporting Information Fig. S2a). BB was vertically homogeneous in most provinces such as NATR_S, NASE_S, ISSG, AUSW, SPSG and PEQD (blue squares, Fig. 4e, Supporting Information Fig. S3d).

The humic-like components C1 and C2 showed a well-defined vertical variability within all provinces, except in NATR_W (Fig. 5a,b, Supporting Information Fig. S2e,f). A significant difference in C1 and C2 above and below the mixed layer was found. The values were lower above the MLD except for PNEC, and very uniform below the mixed layer except in PEQD, NPTG and PNEC (Supporting Information Fig. S2e,f). On the contrary, the amino acid-like components were more homogeneous, showing no variability in most of the provinces situated in the intertropical convergence zone (ITCZ) (e.g., NATR, SPSG, and PEQD). The amino acid-like C3 did not present a defined depth profile in most of the provinces (Fig. 5c, Supporting Information Fig. S2g). Contrary to the humic-like substances, the depth profiles of C4 tended to display higher values at surface than at depth in some provinces (e.g., PNEC in C4, Supporting Information Fig. S2h).

Drivers of FDOM variability

To explore the environmental factors that drive the global distribution of fluorescence PARAFAC components in epipelagic waters of the world ocean we used GAMs to allow testing for the occurrence of non-linear relationships (Fig. 6). Initial examination of the covariability among predictors allowed us to reject N^2, O_2 and NO_3^- out of the analysis (Supporting Information Table S1), thus finally testing a total of eight predictor variables: SWR (daily, weekly and monthly), *S*, θ, D*S*, Dθ, AOU, Chl *a* and BB. The variable that exhibited the largest effect on C1 was AOU followed by Chl *a* (Supporting Information Table S2) with a positive power-law function (Fig. 6a). Inclusion of bacterial abundance (BB) in the model, thus reducing the number of cases from 835 to 473 samples, resulted in a positive linear dependence that increased the variance explained slightly from 72.1% to 73.3%, although the relationships kept the same trends (Fig. 6b), and the variables AOU and Chl *a* still explained most of the variability (Supporting Information Table S2).

Likewise, C2 variability was controlled by the same parameters, with AOU also having the largest influence on this component (Supporting Information Table S2). In this case, the AOU-C2 relationship reached a plateau approximately at 170 μmol kg^{-1} (Fig. 6a). It is remarkable that SWR and BB did not contribute significantly to explain C2 in contrast with C1.

The explained variance for the fluororophores C3 and C4 (ca. 30%) was substantially lower than for the fluorophores C1 and C2 (ca. 75%) (Supporting Information Table S2). C3 variability was mostly controlled by *S* and AOU (Supporting Information Table S2), with θ, D*S* and Chl *a* contributing to explain 33% of the total C3 variability. In this case, the relationship *S*–C3 was linear and positive from $S \sim 35$ and the relationship AOU–C3 shifted from positive to negative at around 170 μmol kg^{-1} (Supporting Information Table S2; Fig. 6a).

C4 variability was mainly explained by *S* and depth (Supporting Information Table S2), and along with temperature, Chl *a*, AOU, θ, Dθ, weekly SWR and D*S* the explained variance was only 27%. In the *S*–C4 relationship, C4 started to increase linearly with *S* for values over $\sim$ 35. The relationship between AOU and C4 was linear and negative all over the AOU range, and contrasts with the relationships of AOU with the other components. Considering BB, we observed a positive relationship with C4 and the explained variance increased up to 28% (Supporting Information Table S2), with *S* and depth remaining as the dominant explanatory variables (Supporting Information Table S2). Noticeably, BB did not contribute significantly to explain the distribution of C3, as was also apparent for C2.

In summary, whereas the environmental factors AOU and Chl *a* explained most of the variability of C1 and C2, the variability of C3 and C4 was mostly explained by *S* and AOU and by *S* and depth, respectively. Whereas the dependence with AOU varied with the components, Chl *a* showed a positive the relationship for all of them. BB only contributed to explain significantly the variability of two (C1 and C4) out of the four PARAFAC components.

Discussion

Comparison of the Malaspina PARAFAC fluorescent components with other studies

All the fluorescence PARAFAC fluorescent components identified in this study have been reported earlier in the oceans and in freshwater environments and compared with a range of directly measured spectra derived from known pure substances submitted to OpenFluor by diverse research groups (Murphy et al. 2014). The statistical similarity between fluorescence spectra was quantified using Tucker's congruence coefficient (TCC) (Tucker 1951), which provides a standardized measure of proportionality of elements in two vectors. Fluorescence spectra, consisting of independent excitation and emission spectra, were considered similar when Tucker congruence exceeded 0.95 on the excitation and emission spectra simultaneously. The results of the

global fluorescence inventory carried out by Jørgensen et al. (2011) revealed for the first time in the oceans the ubiquitous signal of the two humic-like fractions that we found in our study, C1 and C2. As in other marine FDOM studies (e.g., Yamashita et al. 2010, 2015; Jørgensen et al. 2011; Timko et al. 2015), our C1 appeared to be a mixture of the classical humic-like peaks A and C defined by Coble (1996). This component has also been frequently detected in terrestrial and low salinity coastal environments (e.g., identified as C3 in Stedmon et al. 2003 (TCC = 0.98); C4 in Conmy et al. 2004; Stedmon and Markager 2005a; C2 in C3/P3 in Murphy et al. 2008; C3 in Catalá et al. 2013; C2 in Kowalczuk et al. 2013 (TCC = 0.99); Yamashita et al. 2013; C1 in Tanaka et al. 2014 (TCC = 0.99); Wang et al. 2014), as well as in rivers (e.g., C3 in Hong et al. 2005; Chen et al. 2013) or in tropical lakes (C3 in Bittar et al. 2015), boreal aquatic networks (C2 in Lapierre et al. 2014 (TCC = 0.95)) or in a vegetation-free Antarctic lake (Cory and McKnight 2005). C1 is related to the prokaryotic microbial processing of organic matter in both terrestrial and oceanic regions (Romera-Castillo et al. 2010). Our C2 was similar to the marine humic-like components found in other PARAFAC models performed in the ocean (C4 in Stedmon et al. 2003 (TCC = 0.97); C3 in Walker et al. 2009 (TCC = 0.98); C2 in Yamashita et al. 2010; C4 in Jørgensen et al. 2011; C2 in Tanaka et al. 2014 (TCC = 0.96)), as well as others from coastal environments (Murphy et al. 2008; C6 in Yamashita et al. 2008; C1 in Yamashita et al. 2011; Catalá et al. 2013). Similarly, it was also found in rivers and lakes (Cory and McKnight 2005). C2 also represents a group of fluorescent substances associated with microbial activity, but probably more related to eukaryota (Romera-Castillo et al. 2010).

Unlike other studies that found up to four amino acid-like components (e.g., Yamashita et al. 2008; Jørgensen et al. 2011), we only found two amino acid-like C3 and C4, with fluorescence characteristics almost identical to those of free tryptophan and tyrosine (Yamashita and Tanoue 2003b), and also similar to those of tryptophan- (C4 in Stedmon et al. 2007 (TCC = 0.97); C1 in Stedmon et al. 2011 (TCC = 0.97)) and tyrosine-like components found in previous PARAFAC studies either in the ocean (Murphy et al. 2006, 2008; Yamashita et al. 2008) and in coastal or inland waters (Cory and McKnight 2005; Stedmon and Markager 2005a; C5 in Walker et al. 2009 (TCC = 0.97)).

Comparing our four-component PARAFAC model with the first global inventory of seven-component PARAFAC model carried out by Jørgensen et al. (2011), we presume that the exclusive coverage of remote oceanic areas during the Malaspina 2010 expedition resulted in the absence of more fluorescent components characterizing coastal and/or more productive sites. Likely, sampling closer to coastal areas in Jørgensen et al. (2011) allowed them to find two other amino acid-like peaks that were attributed to phenylalanine and to a tyrosine remnant, and a peak with intermediate fluorescence spectrum of the humic- and amino acid-like materials.

Our selection of the four-component PARAFAC model does not mean that the FDOM exclusively contained these four fluorophores, but it is an indicator of the most representative ones in the EEM database. Regarding fluorescence intensities, Jørgensen et al. (2011) and our global FDOM inventories are directly comparable since they are standardized in Raman units (RU). For the case of the four PARAFAC components that we have in common, the intensity ranges are very similar, except for the tryptophan peak that is slightly higher in Jørgensen's et al. study, ranging approximately between below detection limit and 20×10^{-3} RU for the humic-like substances, below detection limit and 40 (up to 60 in Jørgensen's study) $\times 10^{-3}$ RU for the tryptophan peak, and below detection limit and 40×10^{-3} RU for the tyrosine peak.

Humic-like components and their major drivers

The increase with depth of the humic-like FDOM components in the upper 200 m followed the regular pattern previously reported for open ocean waters (Fig. 3) of the Atlantic (Mopper et al. 1991; Chen and Bada 1992; Determann et al. 1996; Kowalczuk et al. 2013; Lønborg et al. 2015; Timko et al. 2015), the Southern ocean (Wedborg et al. 1998; Yamashita et al. 2007), the equatorial Pacific (Chen and Bada 1992; Hayase and Shinozuoka 1995), the Okhotsk Sea and the northwestern North Pacific (Tani et al. 2003; Omori et al. 2010; Yamashita et al. 2010, 2015), the Arabian Sea (Coble et al. 1998) or the global cruise of Jørgensen et al. (2011) that covered the Atlantic, Pacific, Indian, and Southern Oceans. Generally, the humic-like FDOM intensity is lower in surface waters where sunlight penetrates and photolyses the involved compounds, which have been shown to be very vulnerable to natural solar radiation (Omori et al. 2010, 2011). Photobleaching has a significant influence on the optical properties of DOM in the open ocean (Helms et al. 2013) and its vertical effect is limited to the penetration of the ultraviolet radiation in the ocean (Kowalczuk et al. 2013). However, in our study, the weekly SWR does not contribute substantially to explain the fluorescence component profiles and using daily or monthly SWR instead of weekly does not affect the final selection of explanatory variables. We only found a slight negative relationship of weekly SWR with C1 and C4 and monthly SWR with C3 (Fig. 6, Supporting Information Table S2), but not with C2. We presume that the prolonged exposure of surface water bodies to sunlight results in a photobleaching saturation in the oceanic (mostly equatorial and subtropical) regions covered by the Malaspina circumnavigation, thus leading to significant but minor effects with weekly and monthly SWR. Consequently, the photochemical degradation will affect equally in all biogeographic provinces studied regardless of the solar radiation received. In fact, previous irradiation experiments

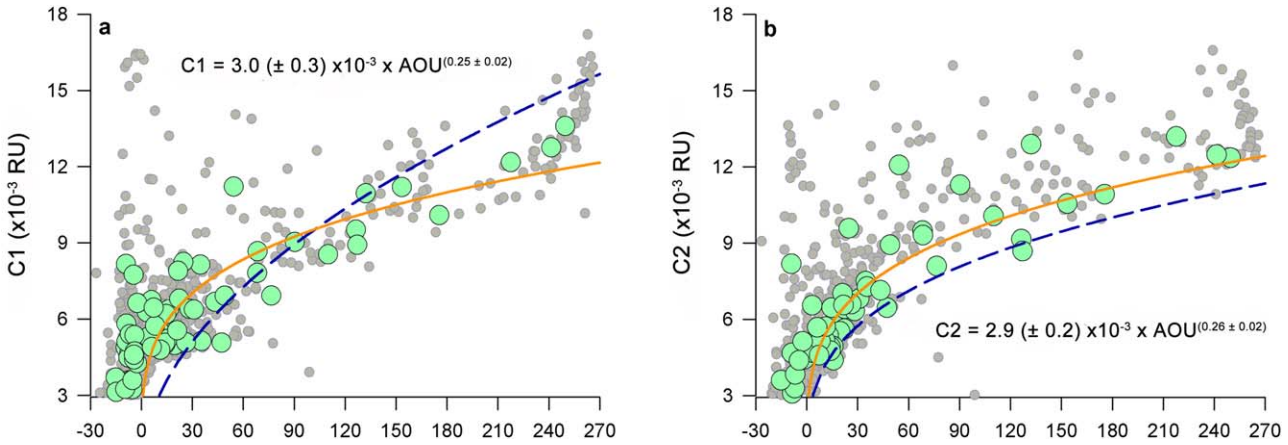

Fig. 7. Relationships between the humic-like fluorescence PARAFAC components and AOU. Measured values (grey dots) and average values (green dots) for each nominal depth level of each province for the components C1 (**a**) and C2 (**b**). The power-law regression curves for the surface (in orange) and for the dark ocean (in dashed blue after Catalá et al. 2015a). AOU-C1: $R^2 = 0.73$, $p < 0.0001$, $n = 45$; AOU-C2: $R^2 = 0.80$, $p < 0.0001$, $n = 45$. Note: the values with AOU < 0 were not considered in the AOU-components relationships.

with natural waters showed the highest humic-like substances depletion rates during the first hours (Del Vecchio and Blough 2002; Nieto-Cid et al. 2006; Timko et al. 2015), then a slowing down after 20 d (Helms et al. 2013). Likewise, the humic-like peak A/C experienced the lowest losses after 24-h irradiation in the surface samples compared with greater depths (Timko et al. 2015), which is likely a result of the highly photodegraded material that was already present.

Remarkably, distinct changes in FDOM composition occurred within and below the upper mixed layer, which limits vertical mixing and thus exposure of DOM to solar radiation to depths shallower than MLD. The DOM below the MLD is characterized by low amino acid-like to humic-like fluorescence intensity ratios. Indeed, we found different responses above and below the MLD for the four fluorescent components (Fig. 3, Supporting Information Fig. S2e–h). This suggests that DOM may consist of more aromatic humic-like compounds produced mostly by bacterial processing of organic matter in the deep ocean (Yamashita and Tanoue 2008; Yamashita et al. 2010). In this regard, the fluorescence intensities of the humic-like components differed between the surface and deep waters during the Malaspina 2010 expedition. The values of the humic-like components C1 and C2 in the surface ocean (< 200 m) were lower than those from the dark ocean. In addition, the large-scale downwelling circulation of the gyres limiting the input of humic-like DOM from deep waters and the solar exposure photobleaching the humic-like fluorescent components jointly create the scenario observed in the subtropical oligotrophic gyres of the South Atlantic, South and North Pacific and South Indian (i.e., SATL, ISSG, SPSG, and NPTG), where the strongest depletion of the humic-like components was found. In our circumnavigation, the minimum values of C1 and C2 at both surface and deep ocean were found in the South Indian Ocean. Regarding the depletion of the humic-like components in surface waters and the increase with depth, Timko et al. (2015) found that in the eastern North Atlantic Ocean and the northern Sargasso Sea, the humic-like C1 and C2 were on average 5.9 and 3.4 times higher below 1000 m than at the surface.

Comparing the geographical distribution of FDOM in this article with that from the dark ocean (> 200 m) during the same circumnavigation (Catalá et al. 2015a), we found that the maximum fluorescence intensities were located in the Equatorial North Pacific. At the surface, the highest values for both C1 and C2 were found in the PNEC province, and in the deep waters in the North Pacific Intermediate Water (NPIW) and in the North Pacific Central Mode Water (CMW_{NP}) (Catalá et al. 2015a). This unique oddity had escaped detection because this region was covered for the first time during the Malaspina cruise (Morel et al. 2010; Yamashita et al. 2010; Jørgensen et al. 2011). The North Atlantic and the Equatorial upwelling regions deviated from the aforementioned increasing depth profile for the humic-like substances and showed the maximum values in the surface (e.g., Jørgensen et al. 2011; Kowalczuk et al. 2013). The reasons behind the high abundance of humic-like materials in upwelling regions are (1) the high microbial productivity in response to nutrient fertilization by deep waters and (2) the net upward advection flux of deep water enriched in humic-like materials (Siegel et al. 2002).

The GAM analysis of the humic-like C1 and C2 indicate that microbial heterotrophic metabolism (AOU as an indicator) and primary production (Chl *a* as an indicator) are the factors that mostly affect the generation of these fluorophores. BB slightly improved the explanatory power of the GAM for C1, whereas its contribution was negligible for C2. It is well known that microbes are directly releasing humic-

like compounds during its metabolism (Romera-Castillo et al. 2010, 2011; Fukuzaki et al. 2014), but also primary production is likely indirectly boosting the C1 humic-like synthesis by generating labile substrates that enhance bacterial growth, thus contributing to the microbial carbon pump (MCP) (Ogawa et al. 2001; Jiao et al. 2010).

Since AOU was the most significant variable explaining C1 and C2, we further explored their relationships to compare them with previous studies (Fig. 7a,b). As in the dark ocean, the AOU–C1 and AOU–C2 relationships were power law, positive and highly significant (Fig. 7). As we were interested in the effect of microbial metabolism on C1 and C2 production, the values in which primary production rates prevails over respiration rates (i.e., AOU < 0 μmol kg^{-1}) were excluded from this comparison. In this way, the effect of primary production and exchange with the atmosphere on the AOU distribution is minimized. Note that the average values per province and depth levels are used to perform these correlations. However, unlike the dark ocean, where the C1 conversion efficiency exceeded that of C2, in the illuminated ocean the conversion efficiencies of both humic-like components were similar. By comparing these regressions with those from the dark ocean (Catalá et al. 2015a), we found that in both cases the exponents were higher in the dark ocean (i.e., 0.51 ± 0.04 for C1 and 0.31 ± 0.04 for C2, respectively), indicating a higher conversion efficiency of the humic-like substances in the dark ocean than in surface waters, where a net effect of photobleaching was also detected.

Amino acid-like components and its major drivers

The decrease of the amino acid-like components with depth suggests that those substances were autochthonously produced and likely more resistant to photobleaching (Determann et al. 1996; Yamashita and Tanoue 2003b; Jørgensen et al. 2011; Guéguen et al. 2012; Helms et al. 2013; Kowalczuk et al. 2013) (Fig. 3c,d). In fact, there appears to be consistent dominance of amino acid-like fluorescence intensity dominance in the surface waters of the Atlantic Meridional Transect (Kowalczuk et al. 2013), the eastern Atlantic Ocean and in the northern Sargasso Sea (Timko et al. 2015) or in the southern Canada Basin and in the East Siberia Sea (Guéguen et al. 2012). Here, we find larger values of the tyrosine-like C4 at the surface than in the dark ocean, with half of the data exceeding 10.2×10^{-3} RU, whereas for the dark ocean half of the data exceeded 4.9×10^{-3} RU. The vertical patterns of both C3 and C4 are similar to those obtained by Jørgensen et al. (2011) and Timko et al. (2015), as they found that tyrosine-like C4 was approximately 1.5 times higher at the surface than in waters > 1000 m depth and that tryptophan-like C3 did not show a clear depth-dependence.

The amino acid-like components showed a positive relationship with Chl *a* for both C3 and C4, and only with BB for C4, which implies a more relevant role of bacteria on the distribution of C4 (Supporting Information Table S2; Fig. 6). The relationship C4–AOU was negative and less significant than for the humic-like components (Supporting Information Table S2; Fig. 6). In the dark ocean, Catalá et al. (2015a) obtained the same result, and explained the negative relationship by the microbial consumption of the more recalcitrant fraction of the amino acid materials represented by this fluorescence signature with a timescale of centuries. In the surface ocean, we are likely observing the bulk of the recently produced tyrosine-like materials that escape rapid microbial utilisation and the negative relationship with AOU would also be a consequence of the microbial utilization of a less recalcitrant fraction of the amino acid-like substances. Similarly, the adverse conditions of the environment might be contributing to the inhibition of the exometabolites (e.g., peptides) released by bacteria typical of quorum sensing (Pereira and Giani 2014). This assumption, as well as the one that involves microbially produced humic-like substances, is supported by a 72 h incubation experiment in the darkness where the amino acid-like fluorescence decayed by $29\% \pm 9\%$ and the marine humic-like fluorescence increased by $20\% \pm 9\%$ (Lønborg et al. 2015). C3 did not show any trend with AOU throughout the whole water column although we saw a shift in the trend from positive to negative at around 170 μmol kg^{-1} due to the subsurface waters of PNEC (Figs. 2a, 6a). However, unlike the dark ocean, we found a positive and significant relationship of the amino acid-like components with salinity ($F_{S\text{-}C3} = 67$ and $F_{S\text{-}C4} = 39$, $p < 0.0001$, Supporting Information Table S2), that could be related to the atmospheric influence within the surface layer. The areas exposed to more intense solar radiation result in both higher water evaporation (i.e., higher salinity) and photobleaching rates of the most sensitive (i.e., humic like components) chromophoric material (Omori et al. 2010, 2011) and likely an accumulation of the less photoreactive (i.e., amino acid-like) components. In addition, as it has been reported that photodegradation shifts the higher molecular weight (MW) materials to lower MW (MW) fractions (Omori et al. 2011, 2015), we could expect that the LMW DOM become more available to microbes that, in turn, could synthesize fresh tryptophan- and tyrosine-like materials.

Conclusions

The relationships between environmental factors and fluorescence PARAFAC components in the epipelagic global ocean are mostly non-linear, which encourages the use of GAMs for describing the large-scale variability of FDOM. GAMs results showed that the environmental drivers of the humic-like and amino acid-like fluorescent components, as well as the robustness of the relationships are not the same, with the humic-like components being primarily affected by microbial activity (AOU and Chl *a*), and the amino acid-like components by physical processes (*S*). Whereas AOU varied

among the four fluorescent components, being positive for the case of the humic-like materials and negative for the tyrosine-like C4, Chl *a* always showed a positive pattern with all the components. Consideration of BB resulted in a minor influence of this variable in C1 and C4.

References

Álvarez, M., and others. 2012. Muestreo y análisis de oxígeno disuelto (O_2) en agua de mar. Expedición de circunnavegación Malaspina 2010: Cambio global y exploración de la biodiversidad del océano. In Libro blanco de métodos y técnicas de trabajo oceanográfico. E. Moreno-Ostos. Madrid, CSIC, p.79–92.

Benson, B. B., and D. Krauss, Jr. 1984. The concentration and isotopic fractionation of oxygen dissolved in freshwater and seawater in equilibrium with the atmosphere. Limnol. Oceanogr. **29**: 620–632. doi:10.4319/lo.1980.25.4.0662

Bittar, T. B., A. Stubbins, A. A. H. Vieira, and K. Mopper. 2015. Characterization and photodegradation of dissolved organic matter (DOM) from a tropical lake and its dominant primary producer, the cyanobacteria *Microcystis aeruginosa*. Mar. Chem. **177**: 205–217. doi:10.1016/j.marchem.2015.06.016

Blasco, D., P. de la Fuente Gamero, and M. Galindo. 2012. Muestreo y análisis de nutrientes inorgánicos disueltos en agua de mar. Expedición de circunnavegación Malaspina 2010: Cambio global y exploración de la biodiversidad del océano. Libro blanco de métodos y técnicas de trabajo oceanográfico. E. Moreno-Ostos. Madrid, CSIC, p. 107–121.

Bricaud, A., M. Babin, H. Claustre, J. Ras, and F. Tièche. 2010. Light absorption properties and absorption budget of Southeast Pacific waters. J. Geophys. Res. **115**: C08009. doi:10.1029/2009JC005517

Calvo-Díaz, A., and X. A. G. Morán. 2006. Seasonal dynamics of picoplankton in shelf waters of the southern Bay of Biscay. Aquat. Microb. Ecol. **42**: 159–174. doi:10.3354/ame042159

Carlson, C. A. 2002. Production and removal processes, p. 91–151. *In* D. A. Hansell and C. A. Carlson [eds.], Biogeochemistry of marine dissolved organic matter. Elsevier. doi:10.1016/B978-012323841-2/50006-3

Carlson, C. A., and D. A. Hansell. 2015. DOM sources, sinks, reactivity and budgets, 2nd ed, p. 65–126. *In* D. A. Hansell and C. A. Carlson [eds.], Biogeochemistry of marine dissolved organic matter. Academic Press. doi:10.1016/B978-0-12-405940-5.00003-0

Catalá, T. S., N. Mladenov, F. Echevarría, and I. Reche. 2013. Positive trends between salinity and chromophoric and fluorescent dissolved organic matter in a seasonally inverse estuary. Estuar. Coast. Shelf Sci. **133**: 206–216. doi:10.1016/j.ecss.2013.08.030

Catalá, T. S., and others. 2015a. Turnover time of fluorescent dissolved organic matter in the dark global ocean. Nat. Commun. **6**: 5986. doi:10.1038/ncomms6986

Catalá, T. S., and others. 2015b. Water mass age and ageing driving chromophoric dissolved organic matter in the dark global ocean. Global Biogeochem. Cycles **29**: 1–18. doi:10.1002/2014GB005048

Chen, R. F., and J. L. Bada. 1992. The fluorescence of dissolved organic matter in seawater. Mar. Chem. **37**: 191–221. doi:10.1016/0304-4203(92)90078-O

Chen, H., W. Meng, B. Zheng, C. Wang, and L. An. 2013. Optical signatures of dissolved organic matter in the watershed of a globally large river (Yangtze River, China). Limnologica **43**: 482–491. doi:10.1016/j.limno.2013.04.004

Coble, P. G. 1996. Characterization of marine and terrestrial DOM in seawater using excitation–emission matrix spectroscopy. Mar. Chem. **51**: 325–346. doi:10.1016/0304-4203(95)00062-3

Coble, P. G. 2007. Marine optical biogeochemistry: The chemistry of ocean color. Chem. Rev. **107**: 402–418. doi:10.1021/cr050350+

Coble, P. G., C. E. Del Castillo, and B. Avril. 1998. Distribution and optical properties of CDOM in the Arabian Sea during the 1995 Southwest Monsoon. Deep-Sea Res. Part II **45**: 2195–2223. doi:10.1016/S0967-0645(98)00068-X

Conmy, R. N., P. G. Coble, R. F. Chen, and G. B. Gardner. 2004. Optical properties of dissolved organic matter in the Northern Gulf of Mexico. Mar. Chem. **89**: 127–144. doi:10.1016/j.marchem.2004.02.010

Cory, R. M., and D. M. McKnight. 2005. Fluorescence spectroscopy reveals ubiquitous presence of oxidized and reduced quinines in dissolved organic matter. Environ. Sci. Technol. **39**: 5142–8149. doi:10.1021/es0506962

Dainard, P. G., and C. Guéguen. 2013. Distribution of PARAFAC modelled CDOM components in the North Pacific Ocean, Bering, Chukchi and Beaufort Seas. Mar. Chem. **157**: 216–223. doi:10.1016/j.marchem.2013.10.007

De La Fuente, P., and others. 2014. Does a general relationship exist between fluorescent dissolved organic matter and microbial respiration?—The case of the dark equatorial Atlantic Ocean. Deep-Sea Res. Part I **89**: 44–55. doi:10.1016/j.dsr.2014.03.007

Del Vecchio, R., and N. V. Blough. 2002. Photobleaching of chromophoric dissolved organic matter in natural waters: Kinetics and modeling. Mar. Chem. **78**: 231–253. doi:10.1016/S0304-4203(02)00036-1

Determann, S., R. Reuter, and R. Willomm. 1996. Fluorescent matter in the eastern Atlantic Ocean. Part 2: Vertical profiles and relation to water masses. Deep-Sea Res. Part I **43**: 345–360. doi:10.1016/0967-0637(96)00008-8

D'Sa, E. J., J. I. Goes, H. Gomes, and D. Mouw. 2014. Absorption and fluorescence properties of CDOM of the eastern Bering Sea. Biogeosciences **11**: 3225–3244. doi:10.5194/bg-11-3225-2014

Ducklow, H. W. 2003. Biogeochemical provinces: Towards a JGOFS synthesis. *In* M. J. R. Fasham [eds.], Ocean biogeochemistry, Berlin.

Estrada, M. 2012. Determinación fluorimétrica de la clorofila a. Expedición de circunnavegación Malaspina 2010: Cambio global y exploración de la biodiversidad del océano. Libro blanco de métodos y técnicas de trabajo oceanográfico. CSIC.

Fellman, J. B., D. V. D'Amore, E. Hood, and R. D. Boone. 2008. Fluorescence characteristics and biodegradability of dissolved organic matter in forest and wetland soils from coastal temperate watersheds in southeast Alaska. Biogeochemistry **88**: 169–184. doi:10.1007/s10533-008-9203-x

Fernández-Castro, B., and others. 2014. Microstructure turbulence and diffusivity parameterization in the tropical and subtropical Atlantic, Pacific and Indian Oceans during the Malaspina 2010 expedition. Deep-Sea Res. Part I **94**: 15–30. doi:10.1016/j.dsr.2014.08.006

Fukuzaki, K., I. Imai, K. Fukushima, K.-I. Ishii, S. Sawayama, and T. Yoshioka. 2014. Fluorescent characteristics of dissolved organic matter produced by bloom-forming coastal phytoplankton. J. Plankton Res. **36**: 685–694. doi:10.1093/plankt/fbu015

Gasol, J. M., and P. A. del Giorgio. 2000. Using flow cytometry for counting natural planktonic bacteria and understanding the structure of planktonic bacterial communities. Sci. Mar. **64**: 197–224. doi:10.3989/scimar.2000.64n2197

Guéguen, C., F. A. McLaughlin, E. C. Carmack, M. Itoh, H. Narita, and S. Nishino. 2012. The nature of colored dissolved organic matter in the southern Canada Basin and East Siberian Sea. Deep-Sea Res. Part II **81–84**: 102–113. doi:10.1016/j.dsr2.2011.05.004

Guéguen, C., C. W. Cuss, C. J. Cassels, and E. C. Carmack. 2014. Absorption and fluorescence of dissolved organic matter in the waters of the Canadian Arctic Archipelago, Baffin Bay, and the Labrador Sea. J. Geophys. Res. Oceans **119**: 2034–2047. doi:10.1002/2013JC009173

Gundersen, K., M. Heldal, S. Norland, D. A. Purdie, and A. H. Knap. 2002. Elemental C, N, and P cell content of individual bacteria collected at the Bermuda Atlantic time-series study (BATS) site. Limnol. Oceanogr. **47**: 1525–1530. doi:10.4319/lo.2002.47.5.1525

Hayase, K., and N. Shinozuka. 1995. Vertical distribution of fluorescent organic matter along with AOU and nutrients in the equatorial Central Pacific. Mar. Chem. **48**: 283–290. doi:10.1016/0304-4203(94)00051-E

Heller, M. I., D. M. Gaiero, and P. L. Croot. 2013. Basin scale survey of marine humic fluorescence in the Atlantic: Relationship to iron solubility and H_2O_2. Global Biogeochem. Cycles **27**: 88–100. doi:10.1029/2012GB004427

Helms, J. R., A. Stubbins, E. M. Perdue, N. W. Green, H. Chen, and K. Mopper. 2013. Photochemical bleaching of oceanic dissolved organic matter and its effect on absorption spectral slope and fluorescence. Mar. Chem. **155**: 81–91. doi:10.1016/j.marchem.2013.05.015

Hong, H., J. Wu, S. Shang, and C. Hu. 2005. Absorption and fluorescence of chromophoric dissolved organic matter in the Pearl River Estuary, South China. Mar. Chem. **97**: 78–89. doi:10.1016/j.marchem.2005.01.008

Hudson, N., A. Baker, and D. Reynolds. 2007. Fluorescence analysis of dissolved organic matter in natural, waste and polluted waters—A review. River Res. Appl. **23**: 631–649. doi:10.1002/rra.1005

Jiao, N., and others. 2010. Microbial production of recalcitrant dissolved organic matter: Long-term carbon storage in the global ocean. Nat. Rev. Microbiol. **8**: 593–599. doi:10.1038/nrmicro2386

Jørgensen, L., and others. 2011. Global trends in the fluorescence characteristics and distribution of marine dissolved organic matter. Mar. Chem. **126**: 139–148. doi:10.1016/j.marchem.2011.05.002

Jørgensen, L., C. A. Stedmon, M. A. Granskog, and M. Middelboe. 2014. Tracing the long-term microbial production of recalcitrant fluorescent dissolved organic matter in seawater. Geophys. Res. Lett. **41**: 2481–2488. doi:10.1002/2014GL059428

Kaiser, K., and R. Benner. 2009. Biochemical composition and size distribution of organic matter at the Pacific and Atlantic time-series stations. Mar. Chem. **113**: 63–77. doi:10.1016/j.marchem.2008.12.004

Kalle, K. 1949. Fluorescence and contents of yellow substance in the Gulfs of Bothnia and Finland. Deutsche Hydrographische Zeitschrift **2**: 9–124.

Kieber, D. J., J. McDaniel, and K. Mopper. 1989. Photochemical source of biological substrates in sea water: Implications for carbon cycling. Nature **341**: 637–369. doi:10.1038/341637a0

Kieber, R. J., L. H. Hydro, and P. J. Seaton. 1997. Photooxidation of triglycerides and fatty acids in seawater: Implication toward the formation of marine humic substances. Limnol. Oceanogr. **42**: 1454–1462. doi:10.4319/lo.1997.42.6.1454

Kim, J., and G. Kim. 2015. Importance of colored dissolved organic matter (CDOM) inputs from the deep sea to the euphotic zone: Results from the East (Japan) Sea. Mar. Chem. **169**: 33–40. doi:10.1016/j.marchem.2014.12.010

Kowalczuk, P., G. H. Tilstone, M. Zablocka, R. Röttgers, and R. Thomas. 2013. Composition of dissolved organic matter along an Atlantic meridional transect from fluorescence spectroscopy and parallel factor analysis. Mar. Chem. **157**: 170–184. doi:10.1016/j.marchem.2013.10.004

Lønborg, C., T. Yokokawa, G. J. Herndl, and X. A. Álvarez-Salgado. 2015. Production and degradation of fluorescent dissolved organic matter in surface waters of the eastern north Atlantic ocean. Deep-Sea Res. Part I **96**: 28–37. doi:10.1016/j.dsr.2014.11.001

Longhurst, A. 1995. Seasonal cycles of pelagic production and consumption. Prog. Oceanogr. **36**: 77–167. doi:10.1016/0079-6611(95)00015-1

Longhurst, A. R. 1998. Ecological geography of the sea. Academic Press.

Maie, N., Y. Yamashita, R. M. Cory, J. N. Boyer, and R. Jaffé. 2012. Application of excitation emission matrix fluorescence monitoring in the assessment of spatial and seasonal drivers of dissolved organic matter composition: Sources and physical disturbance controls. Appl. Geochem. **27**: 917–929. doi:10.1016/j.apgeochem.2011.12.021

Millard, R. C., W. B. Owens, and N. P. Fofonoff. 1990. On the calculation of the Brunt-Väisälä frequency. Deep-Sea Res. **37**: 167–181. doi:10.1016/0198-0149(90)90035-T

Miller, W. L., and R. G. Zepp. 1995. Photochemical production of dissolved inorganic carbon from terrestrial organic matter: Significance to the oceanic organic carbon cycle. Geophys. Res. Lett. **22**: 417–420. doi:10.1029/94GL03344

Mopper, K., X. L. Zhou, R. J. Kieber, D. J. Kieber, R. J. Sikorski, and R. D. Jones. 1991. Photochemical degradation of dissolved organic carbon and its impact on the oceanic carbon cycle. Nature **353**: 60–62. doi:10.1038/353060a0

Moran, M. A., and R. G. Zepp. 1997. Role of photoreactions in the formation of biologically labile compounds from dissolved organic matter. Limnol. Oceanogr. **42**: 1307–1316. doi:10.4319/lo.1997.42.6.1307

Morel, A., B. Gentili, H. Claustre, M. Babin, A. Bricaud, J. Ras, and F. Tièche. 2007. Optical properties of the "clearest" natural waters. Limnol. Oceanogr. **52**: 217–229. doi:10.4319/lo.2007.52.1.0217

Morel, A., and B. Gentili. 2009. A simple band ratio technique to quantify the colored dissolved and detrital organic material from ocean color remotely sensed data. Remote Sens. Environ. **113**: 998–1011. doi:10.1016/j.rse.2009.01.008

Morel, A., H. Claustre, and B. Gentili. 2010. The most oligotrophic subtropical zones of the global ocean: Similarities and differences in terms of chlorophyll and yellow substance. Biogeosciences **7**: 3139–3151. doi:10.5194/bg-7-3139-2010

Murphy, K. R., G. M. Ruiz, W. T. M. Dunsmuir, and T. D. Waite. 2006. Optimized parameters for fluorescence-based verification of ballast water exchange by ships. Environ. Sci. Technol. **40**: 2357–2362. doi:10.1021/es0519381

Murphy, K. R., C. A. Stedmon, T. D. Waite, and G. M. Ruiz. 2008. Distinguishing between terrestrial and autochthonous organic matter sources in marine environments using fluorescence spectroscopy. Mar. Chem. **108**: 40–58. doi:10.1016/j.marchem.2007.10.003

Murphy, K. R., and others. 2010. Measurement of dissolved organic matter fluorescence in aquatic environments: An interlaboratory comparison. Environ. Sci. Technol. **44**: 9405–9412. doi:10.1021/es102362t

Murphy, K. R., C. A. Stedmon, D. Graeber, and R. Bro. 2013. Fluorescence spectroscopy and multi-way techniques. PARAFAC. Anal. Methods **5**: 6557–6566. doi:10.1039/c3ay41160e

Murphy, K. R., C. A. Stedmon, P. Wenig, and R. Bro. 2014. OpenFluor- an online spectral library of autofluorescence by organic compounds in the environment. Anal. Methods **6**: 658–661. doi:10.1039/C3AY41935E

Nelson, N. B., D. A. Siegel, and A. F. Michaels. 1998. Seasonal dynamics of colored dissolved material in the Sargasso Sea. Deep-Sea Res. Part I **45**: 931–957. doi:10.1016/S0967-0637(97)00106-4

Nelson, N. B., and D. A. Siegel. 2002. Chromophoric DOM in the open ocean, p. 547–578. *In* D. A. Hansell and C. A. Carlson [eds.], Biogeochemistry of marine dissolved organic matter. Academic Press. doi:10.1016/B978-012323841-2/50013-0

Nelson, N. B., and D. A. Siegel. 2013. The global distribution and dynamics ofchromophoric dissolved organic matter. Ann. Rev. Mar. Sci. **5**: 447–476. doi:10.1146/annurev-marine-120710-100751

Nieto-Cid, M., Álvarez-Salgado, X. A., Pérez, F. F. 2006. Microbial and photochemical reactivity of fluorescent dissolved organic matter in a coastal upwelling system. Limnol. Oceanogr., **51**: 1391–1400.

Ogawa, H., Y. Amagai, I. Koike, K. Kaiser, and R. Benner. 2001. Production of refractory dissolved organic matter by bacteria. Science **292**: 917–920. doi:10.1126/science.1057627

Omori, Y., T. Hama, M. Ishii, and S. Saito. 2010. Relationship between the seasonal change in fluorescent dissolved organic matter and mixed layer depth in the subtropical western North Pacific. J. Geophys. Res. **115**: C06001. doi:10.1029/2009JC005526

Omori, Y., T. Hama, M. Ishii, and S. Saito. 2011. Vertical change in the composition of marine humic-like fluorescent dissolved organic matter in the subtropical western North Pacific and its relation to photoreactivity. Mar. Chem. **124**: 38–47. doi:10.1016/j.marchem.2010.11.005

Omori, Y., T. Hama, and M. Ishii. 2015. Photochemical bleaching of fluorescent dissolved organic matter in the subtropical North Pacific Ocean. Geochem. J. **49**: 175–184. doi:10.2343/geochemj.2.0343

Ortega-Retuerta, E., T. K. Frazer, C. M. Duarte, S. Ruiz-Halpern, A. Tovar-Sánchez, J. M. Arrieta, and I. Reche. 2009. Biogeneration of chromophoric dissolved organic matter by bacteria and krill in the Southern Ocean. Limnol. Oceanogr. **54**: 1941–1950. doi:10.4319/lo.2009.54.6.1941

Ortega-Retuerta, E., D. A. Siegel, N. B. Nelson, C. M. Duarte, and I. Reche. 2010. Observations of chromophoric dissolved and detrital organic matter distribution using remote sensing in the Southern Ocean: Validation, dynamics and regulation. J. Mar. Syst. **82**: 295–303. doi:10.1016/j.jmarsys.2010.06.004

Pereira, D. A., and A. Giani. 2014. Cell density-dependent oligopeptide production in cyanobacterial strains. FEMS Microbiol. Ecol. **88**: 175–183. doi:10.1111/1574-6941.12281

Pérez-Hernández, M. D., M. Nuez de la Fuente, P. Vélez Belchi, V. M. Benitez Barrios, F. López Laatzen, and E. Fraile Nuez. 2012. Análisis de muestras de salinidad. Salinómetro de laboratorio Autosal 8400B. Expedición de circunnavegación

Malaspina 2010: Cambio global y exploración de la biodiversidad del océano. Libro blanco de métodos y técnicas de trabajo oceanográfico. CSIC, p. 67–76.

R Development Core Team. 2014. R: A language and environment for statistical computing. *In* R Foundation for Statistical Computing, Vienna, Austria. ISBN 3-900051-07-0, http://R-project.org.

Reche, I., E. Pulido-Villena, J. M. Conde-Porcuna, and P. Carrillo. 2001. Photoreactivity of dissolved organic matter from high-mountain lakes of Sierra Nevada, Spain. Arct. Antarct. Alp. Res. **33**: 426–434. doi:10.2307/1552552

Romera-Castillo, C., H. Sarmento, X. A. Álvarez-Salgado, J. M. Gasol, and C. Marrasé. 2010. Production of chromophoric dissolved organic matter by marine phytoplankton. Limnol. Oceanogr. **55**: 446–454. doi:10.4319/lo.2010.55.1.0446

Romera-Castillo, C., H. M. Sarmento, X. A. Álvarez-Salgado, J. M. Gasol, and C. Marrasé. 2011. Net production and consumption of fluorescent colored dissolved organic matter by natural bacterial assemblages growing on marine phytoplankton exudates. Appl. Environ. Microbiol. **77** (21): 7490–7498. doi:10.1128/AEM.00200-11

Siegel, D. A., A. F. Michaels, J. C. Sorensen, M. O'Brien, and M. A. Hammer. 1995. Seasonal variability of light availability and utilization in the Sargasso Sea. J. Geophys. Res. **100**: 8675–8713. doi:10.1029/95JC00447

Siegel, D. A., S. Maritorena, N. B. Nelson, D. A. Hansell, and M. Lorenzi-Kayser. 2002. Global distribution and dynamics of colored dissolved and detrital organic materials. J. Geophys. Res. **107**: 3228. doi:10.1029/2001JC000965

Siegel, D. A., S. Maritorena, N. B. Nelson, M. J. Behrenfeld, and C. R. McClain. 2005. Colored dissolved organic matter and its influence on the satellite-based characterization of the ocean biosphere. Geophys. Res. Lett. **32**: L20605. doi:10.1029/2005GL024310

Stedmon, C. A., and S. Markager. 2003. Behaviour of the optical properties of coloured dissolved organic matter under conservative mixing. Estuar. Coast. Shelf Sci. **57**: 973–979. doi:10.1016/S0272-7714(03)00003-9

Stedmon, C. A., S. Markager, and R. Bro. 2003. Tracing dissolved organic matter in aquatic environments using a new approach to fluorescence spectroscopy. Mar. Chem. **82**: 239–254. doi:10.1016/S0304-4203(03)00072-0

Stedmon, C. A., and S. Markager. 2005a. Resolving the variability in dissolved organic matter fluorescence in a temperate estuary and its catchment using PARAFAC analysis. Limnol. Oceanogr. **50**: 686–697. doi:10.4319/lo.2005.50.2.0686

Stedmon, C. A., and S. Markager. 2005b. Tracing the production and degradation of autochthonous fractions of dissolved organic matter by fluorescence analysis. Limnol. Oceanogr. **50**: 1415–1426. doi:10.4319/lo.2005.50.5.1415

Stedmon, C. A., D. N. Thomas, M. Granskog, H. Kaartokallio, S. Papadimitriou, and H. Kuosa. 2007. Characteristics of dissolved organic matter in baltic coastal sea ice: Allochthonous or autochthonous origins? Global J. Environ. Sci. Technol. **41**: 7273–7279. doi:10.1021/es071210f

Stedmon, C. A., and R. Bro. 2008. Characterizing dissolved organic matter fluorescence with parallel factor analysis: A tutorial. Limnol. Oceanogr.: Methods **6**: 572–579. doi:10.4319/lom.2008.6.572b

Stedmon, C. A., D. N. Thomas, S. Papadimitriou, M. A. Granskog, and G. Dieckmann. 2011. Using fluorescence to characterize dissolved organic matter in Antarctic sea ice brines. J. Geophys. Res. **116**: 1–9. doi:10.1029/2011JG001716

Stedmon, C. A., and N. B. Nelson. 2015. The optical properties of DOM in the ocean, 2nd ed. pp 481–508. *In* D. A. Hansell and C. A. Carlson [eds.], Biogeochemistry of marine dissolved organic matter. Academic Press.

Steinberg, D. K., N. B. Nelson, C. A. Carlson, and A. C. Prusak. 2004. Production of chromophoric dissolved organic matter (CDOM) in the open ocean by zooplankton and the colonial cyanobacterium *Trichodesmium* spp. Mar. Ecol. Prog. Ser. **267**: 45–56. doi:10.3354/meps267045

Suttle, C. A. 2007. Marine viruses—Major players in the global ecosystem. Nat. Rev. Microbiol. **5**: 801–812. doi:10.1038/nrmicro1750

Tanaka, K., K. Kuma, K. Hamasaki, and Y. Yamashita. 2014. Accumulation of humic-like fluorescent dissolved organic matter in the Japan Sea. Sci. Rep. **4**: 5292. doi:10.1038/srep05292

Tani, H., J. Nishioka, K. Kuma, H. Takata, Y. Yamashita, E. Tanoue, and T. Midorikaw. 2003. Iron(III) hydroxide solubility and humic-type fluorescent organic matter in the deep water column of the Okhotsk Sea and the northwestern North Pacific Ocean. Deep-Sea Res. Part I **50**: 1063–1078. doi:10.1016/S0967-0637(03)00098-0

Tedetti, M., B. Charriére, A. Bricaud, J. Para, P. Raimbault, and R. Sempére. 2010. Distribution of normalized water-leaving radiances at UV and visible wave bands in relation with chlorophyll a and colored detrital matter content in the southeast Pacific. J. Geophys. Res. **115**: C02010. doi:10.1029/2009JC005289

Timko, S. A., and others. 2015. Depth-dependent photodegradation of marine dissolved organic matter. Front. Mar. Sci. **2**: 66. doi:10.3389/fmars.2015.00066

Tucker, L. R. 1951. A method for synthesis of factor analysis studies (Personnel Research Section Report No. 984), Department of the Army, Washington D.C., Washington D.C.

Walker, S. A., R. M. W. Amon, C. Stedmon, S. Duan, and P. Louchouarn. 2009. The use of PARAFAC modeling to trace terrestrial DOM and fingerprint water masses in coastal Canadian Arctic surface waters. J. Geophys. Res. Biogeosci. **114**: G00F06. doi:10.1029/2009JG000990

Wang, Y., D. Zhang, Z. Shen, J. Chen, and C. Feng. 2014. Characterization and spatial distribution variability of chromophoric dissolved organic matter (CDOM) in the

Yangtze Estuary. Chemosphere **95**: 353–362. doi:10.1016/j.chemosphere.2013.09.044

Wedborg M., Hoppema M., Skoog A., 1998. On the relation between organic and inorganic carbon in the Weddell Sea. Journal of Marine Systems **17**: 59–76.

Wood, S. 2006. Generalized additive models: An introduction with R. Chapman & Hall.

Yamashita, Y., and E. Tanoue. 2003a. Chemical characterization of protein-like fluorophores in DOM in relation to aromatic amino acids. Mar. Chem. **82**: 255–271. doi:10.1016/S0304-4203(03)00073-2

Yamashita, Y., and E. Tanoue. 2003b. Distribution and alteration of amino acids in bulk DOM along a transect from bay to oceanic waters. Mar. Chem. **82**: 145–160. doi:10.1016/S0304-4203(03)00049-5

Yamashita, Y., A. Tsujasaki, T. Nishida, and E. Tanoue. 2007. Vertical and horizontal distribution of fluorescent dissolved organic matter in the Southern Ocean. Mar. Chem. **106**: 498–509. doi:10.1016/j.marchem.2007.05.004

Yamashita, Y., R. Jaffé, N. Maie, and E. Tanoue. 2008. Assessing the dynamics of dissolved organic matter (DOM) in coastal environments by excitation and emission matrix fluorescence and parallel factor analysis (EEM-PARAFAC). Limnol. Oceanogr. **53**: 1900–1908. doi:10.4319/lo.2008.53.5.1900

Yamashita, Y., and E. Tanoue. 2008. Production of bio-refractory fluorescent dissolved organic matter in the ocean interior. Nat. Geosci. **1**: 579–582. doi:10.1038/ngeo279

Yamashita, Y., R. M. Cory, J. Nishioka, K. Kuma, E. Tanoue, and R. Jaffé. 2010. Fluorescence characteristics of dissolved organic matter in the deep waters of the Okhotsk Sea and the northwestern North Pacific Ocean. Deep-Sea Res. Part II **57**: 1478–1485. doi:10.1016/j.dsr2.2010.02.016

Yamashita, Y., A. Panton, C. Mahaffey, and R. Jaffe. 2011. Assessing the spatial and temporal variability of dissolved organic matter in Liverpool Bay using excitation_emission matrix fluorescence and parallel factor analysis. Ocean Dyn. **61**: 569–579. doi:10.1007/s10236-010-0365-4

Yamashita, Y., J. N. Boyer, and R. Jaffé. 2013. Evaluating the distribution of terrestrial dissolved organic matter in a complex coastal ecosystem using fluorescence spectroscopy. Cont. Shelf Res. **66**: 136–144. doi:10.1016/j.csr.2013.06.010

Yamashita, Y., C.-J. Lu, H. Ogawa, J. Nishioka, H. Obata, and H. Saito. 2015. Application of an in situ fluorometer to determine the distribution of fluorescent organic matter in the open ocean. Mar. Chem. **177**: 298–305. doi:10.1016/j.marchem.2015.06.025

Acknowledgments

We thank C.M. Duarte for the coordination of the Malaspina expedition; the chief scientists of the seven legs, the staff of the Marine Technology Unit (CSIC-UTM) and the Captain and crew of R/V *Hespérides* for their outright support during the circumnavigation. Also, we thank the Physics block for collecting, calibrating and processing the CTD data. Dolors Blasco for facilitating the nutrients data. T.S.C acknowledges funding through a predoctoral fellowship (reference AP2009-2138) from the Ministerio de Educación, Cultura y Deporte. A. Fuentes-Lema and E. Ortega- Retuerta for their contribution to sampling collection and measurements. A. Gomes for coordinating the bacterial analyses. J. Otero was supported by "Junta para la Ampliación de Estudios" Fellowship (JAE-Doc program 2011) from the CSIC and ESF. M. Nieto-Cid was funded by the EU FP/-IOF project FeBOL-220172 and the CSIC Program "Junta para la Ampliación de Estudios" co-financed by the ESF. B. Horstkotte was supported by JAE 2010 Postdoctoral fellowship from the CSIC. This study was financed by the Malaspina 2010 circumnavigation expedition (grant number CSD2008–00077).

Submitted 2 December 2015
Revised 25 January 2016
Accepted 26 January 2016

Associate editor: Ronnie Glud